Monthly Notices
of the
ROYAL ASTRONOMICAL SOCIETY

MNRAS **495,** 3859–3880 (2020)
Advance Access publication 2020 May 15

doi:10.1093/mnras/staa1319

See Change: VLT spectroscopy of a sample of high-redshift Type Ia supernova host galaxies

S. C. Williams [1,2,3]★ I. M. Hook,[1] B. Hayden,[4,5,6] J. Nordin,[7] G. Aldering,[4] K. Boone,[4,5,8] A. Goobar [9], C. E. Lidman [10], S. Perlmutter,[4,5] D. Rubin,[4,6] P. Ruiz-Lapuente,[11,12] C. Saunders[4,13,14] and (The Supernova Cosmology Project)

Affiliations are listed at the end of the paper

Accepted 2020 May 1. Received 2020 April 27; in original form 2019 June 21

ABSTRACT

The Supernova Cosmology Project has conducted the 'See Change' programme, aimed at discovering and observing high-redshift ($1.13 \leq z \leq 1.75$) Type Ia supernovae (SNe Ia). We used multifilter *Hubble Space Telescope* (*HST*) observations of massive galaxy clusters with sufficient cadence to make the observed SN Ia light curves suitable for a cosmological probe of dark energy at $z > 0.5$. This See Change sample of SNe Ia with multi-colour light curves will be the largest to date at these redshifts. As part of the See Change programme, we obtained ground-based spectroscopy of each discovered transient and/or its host galaxy. Here, we present Very Large Telescope (VLT) spectra of See Change transient host galaxies, deriving their redshifts, and host parameters such as stellar mass and star formation rate. Of the 39 See Change transients/hosts that were observed with the VLT, we successfully determined the redshift for 26, including 15 SNe Ia at $z > 0.97$. We show that even in passive environments, it is possible to recover secure redshifts for the majority of SN hosts out to $z = 1.5$. We find that with typical exposure times of 3−4 h on an 8-m-class telescope we can recover ∼75 per cent of SN Ia redshifts in the range of $0.97 < z < 1.5$. Furthermore, we show that the combination of *HST* photometry and VLT spectroscopy is able to provide estimates of host galaxy stellar mass that are sufficiently accurate for use in a mass-step correction in the cosmological analysis.

Key words: techniques: spectroscopic – transients: supernovae – galaxies: clusters: general – galaxies: clusters: individual (MOO J1014+0038, SPT-CL J0205–5829, SPT-CL J2040–4451, SPT-CL J2106–5844) – galaxies: distances and redshifts.

1 INTRODUCTION

Observations of Type Ia supernovae (SNe Ia) at different redshifts by Riess et al. (1998) and Perlmutter et al. (1999) provided the first evidence that the expansion of the Universe is accelerating. Since those works, the number of SNe Ia with high-quality, multicolour light curves has increased enormously at redshifts $z < 1$, from surveys such as ESSENCE (Miknaitis et al. 2007), Supernova Legacy Survey (Guy et al. 2010), Carnegie Supernova Project (Stritzinger et al. 2011), *Hubble Space Telescope* (*HST*) Cluster Supernova Survey (Suzuki et al. 2012), Lick Observatory Supernova Search (Ganeshalingam, Li & Filippenko 2013), Sloan Digital Sky Survey-II (Sako et al. 2018), Pan-STARRS 1 (PS1; Scolnic et al. 2018), and the Dark Energy Survey (Abbott et al. 2019).

Scolnic et al. (2018) combined PS1 SNe Ia with those from several other surveys to produce the 'Pantheon Sample' of 1048 SNe Ia at $0.01 < z < 2.3$. When combined with cosmic microwave background constraints, the sample gave a measurement of a constant dark energy equation of state parameter, $w = -1.026 \pm 0.041$, consistent with the cosmological constant value of $w = -1$. At $z \geq 1$, the SN Ia *Hubble* diagram is still relatively poorly populated, meaning that for SNe Ia, the dark energy equation of state is effectively unconstrained at $z > 0.5$. As the accelerating expansion is not understood, it is important to measure the equation of state of the dark energy component of the Universe to better understand its nature. Measuring w at high-z is important because any deviation from −1 or variation with time would imply that dark energy cannot be in the form of the cosmological constant.

The peak optical luminosities of SNe Ia are strongly correlated with the width of their light curves, with more luminous SNe Ia having broader light curves. This allows the width of the light curve to be used to standardize the peak absolute brightness of individual

★ E-mail: steven.williams@utu.fi

SNe Ia (Phillips 1993). A correction for the SN colour further reduces the scatter in the standardized brightnesses (Riess, Press & Kirshner 1996; Tripp 1998). After corrections for light-curve width (or 'stretch') and colour, there is typically an intrinsic scatter in the Hubble (1929) diagram of $\lesssim$0.15 mag. This, in conjunction with their high luminosities (typically peaking at around $M_B = -19$), is what makes SNe Ia good distance indicators and probes of dark energy.

The observed properties of SNe Ia vary with the nature of their host galaxies. SNe Ia occurring in star-forming disc galaxies tend to be slower declining and more luminous than those in passive early-type galaxies (Hamuy et al. 1995; Sullivan et al. 2006). Even after standardization of the SN Ia light curves using stretch and colour, a correlation between Hubble residual and host galaxy type remains. The Hubble residual of an SN Ia is the offset of its standardized brightness from the expected standardized brightness for SNe Ia (i.e. improved standardization of the SNe would yield smaller Hubble residuals). Standardized SNe Ia in passive galaxies have Hubble residuals that are slightly brighter than those in younger environments (Hicken et al. 2009; Neill et al. 2009). A similar relationship is observed with host galaxy stellar mass, where the standardized brightnesses of SNe Ia occurring in massive galaxies tend to be brighter than those occurring in galaxies with a lower stellar mass (Sullivan et al. 2010). Hubble residuals have also shown to be correlated with the local environment of SNe Ia. After stretch and colour standardization, Rigault et al. (2013) found that SNe Ia with local (within 1 kpc of the SN position) Hα emission were 0.094 $\pm$ 0.031 mag fainter than those from passive regions. Correlations have been found between local specific star formation rate (sSFR) and Hubble residuals (Rigault et al. 2018), and between local colour and Hubble residuals (Roman et al. 2018). For example, Roman et al. (2018) found a systematic difference of 0.091 $\pm$ 0.013 mag between the standardized peak magnitudes of SNe Ia that have a bluer local $U - V$ host colour and those with a redder $U - V$ colour. Hubble residuals may correlate more strongly with local host-galaxy information than they do with global host galaxy properties (Roman et al. 2018). Jones et al. (2018) found that local properties did tend to correlate more strongly with distance residuals, compared to random locations in the SN host galaxy; however, the significance of this difference was relatively low. These works show that host galaxy (and ideally maybe even local) information is an important consideration when doing precision cosmology.

1.1 The See Change survey

The Supernova Cosmology Project has conducted the 'See Change' survey, an extensive space and ground-based observing programme to efficiently discover very high-redshift SNe Ia at $z \geq 1$, with the aim of obtaining a measurement of the dark energy density at $0.5 < z < 1$ that is independent of any assumption regarding the redshift continuity (e.g. via an equation of state parametrization) of dark energy. A detailed overview of the See Change survey will be given by Hayden et al. (in preparation). Observing these very high-redshift SNe Ia probes dark energy at the time the Universe is thought to have transitioned from being matter-dominated to dark-energy dominated. The See Change survey was based on a two-year, 174-orbit *HST* programme (PI: Perlmutter; Program IDs: 13677 and 14327) to observe large galaxy clusters at $1.13 \leq z \leq 1.75$, with the aim of discovering cluster-SNe Ia, and obtaining the high-cadence, multicolour light curves needed for cosmology. Four orbits were also used from *HST* Program 13747 (PI: Tracy Webb). Targeting large galaxy clusters gives many more galaxies in the relatively small field of view (FoV) of *HST* WFC3 than can be achieved in the general field. It also takes advantage of the potentially higher SN Ia rate in clusters at higher redshift, compared to clusters in the local universe (Barbary et al. 2012). One of the cosmological aims of See Change was also to make weak-lensing measurements (e.g. Jee et al. 2017). See Change has also yielded, or contributed to, a number of galaxy cluster studies (e.g. Gonzalez et al. 2015; Webb et al. 2015; Delahaye et al. 2017; Noble et al. 2017; Foltz et al. 2018; Wu et al. 2018; Gonzalez et al. 2019).

The *HST* component of the See Change survey has been supported by several large ground-based spectroscopic follow-up programmes on the Very Large Telescope (VLT), W. M. Keck Observatory (Keck), Gemini Telescopes, Gran Telescopio Canarias (GTC) and *Subaru* Telescope. This spectroscopy is required to determine precise redshifts for the host galaxies of the cosmological SN Ia sample. Obtaining spectroscopic redshifts for these SNe Ia is vital if we are to optimize the power that the See Change sample of SNe Ia has on constraining the cosmology. It is also important to help determine the SN type. In the majority of cases, live SN spectroscopy to determine type was not feasible due to the faintness of the SNe or difficulties in obtaining spectra when the SNe were near maximum light. Most of the transients therefore had to be classified photometrically. Photometric classification of SNe uses the light curves in all available filters to constrain the possible type of a given SN (see e.g. Poznanski et al. 2002). In this method of classification, determination of the precise redshift of the SN removes an important free parameter from the fitting model. This can often break degeneracies arising from the photometry alone, for example, between a lower redshift SN CC and a higher redshift SN Ia.

On overview of the See Change survey will be presented by Hayden et al. (in preparation). Rubin et al. (2018) presented the See Change discovery and observations of a lensed SN Ia at $z = 2.22$. The See Change cosmological analysis will be presented by Hayden et al. (in preparation).

1.2 This work

Here, we present ground-based VLT spectroscopy of the host-galaxies of SN candidates discovered with *HST* during the See Change survey. We also obtained a live spectrum for an active transient with no detected host galaxy, found in the field of the MOO J1014+0038 cluster. In this work, we use the host-galaxy spectra to obtain a precise redshift for each individual transient, which will be used in the cosmological analysis to be published by Hayden et al. (in preparation). The redshifts have also assisted the photometric classification of each transient, as they were often able to break degeneracies in the typing that still remain when considering the (relatively uncertain) photometric redshifts only. The See Change redshift range of $1.13 \leq z \leq 1.75$ prohibits detailed analysis of the local environments of the SNe Ia, even when using *HST*. Using a combination of our VLT spectra and *HST* photometry of the SN Ia host galaxies, we can, however, look at the global host properties, including stellar mass, star formation rate (SFR), and stellar age. The main aim of this part of the work was to obtain the best possible constraints for the stellar mass of each SN Ia host galaxy. This stellar mass measurement can then be used to 'correct' the standardized peak SN Ia brightnesses for the Hubble residual–stellar mass correlation discussed earlier. Given See Change is observing galaxy clusters, the average host galaxy properties are likely to be different from

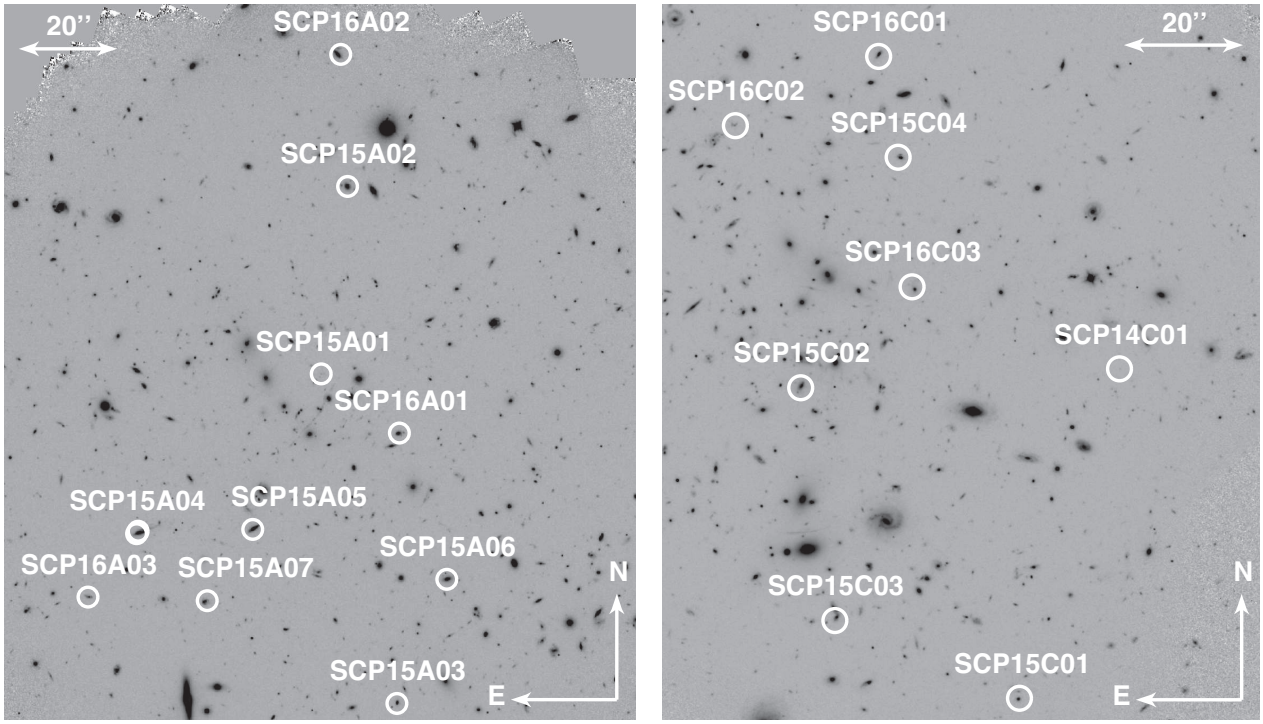

Figure 1. Stacked *HST* WFC3/IR *F*105*W* See Change image of clusters SPT0205 (left-hand panel) and MOO1014 (right-hand panel), with the positions of all transients discovered through the See Change programme indicated. A square-root flux scale is used to aid the visualization of the faint objects. The galaxy that hosted SCP15A04, also produced SCP16A04, hence there are two circles appearing close together in the figure.

those of field SN Ia surveys for example, and therefore the results of this work will be important to consider for the cosmological analysis.

This paper is structured as follows: we give a brief overview of the galaxy clusters for which we obtained VLT data as part of See Change in Section 2. The identification of VLT targets and transient classification is discussed in Section 3. The VLT data and the data reduction are described in Sections 4 and 5, respectively. We describe how we determined the redshifts and galaxy parameters in Sections 6 and 7, before presenting the spectra themselves in Section 8. We then discuss our results, how the host galaxies compare to other galaxy cluster members, and how well our results constrain the galaxy parameters in Section 9, before summarizing the work in Section 10.

2 TARGET CLUSTERS

The See Change programme targeted 12 of the most massive known clusters in the redshift range of $1.13 \leq z \leq 1.75$. An overview of the cluster selection will be presented in Hayden et al. (in preparation). The seven clusters targeted with the VLT observations are briefly discussed below.

The South Pole Telescope (SPT) Survey is a survey to discover galaxy clusters through the Sunyaev–Zel'dovich effect covering 2500 deg^2 of the southern sky (Bleem et al. 2015). Three clusters discovered by this survey were observed as part of See Change: SPT-CL J0205–5829 (hereafter SPT0205) is a massive cluster at $z = 1.32$ identified by Reichardt et al. (2013). It has properties similar to lower redshift clusters of similar mass and Stalder et al. (2013) conclude that the majority of star formation in the cluster occurred at $z > 2.5$. The stacked *HST* image of this cluster, along with the positions of the transients discovered during See Change are shown in Fig. 1. SPT-CL J2106–5844 (hereafter SPT2106) is the most massive cluster known at $z > 1$ (Foley et al. 2011). The *HST* image of this cluster, along with the positions of the transients discovered during See Change are shown in Fig. 2. SPT-CL J2040–4451 (hereafter SPT2040) was discovered by the SPT–SZ survey (Reichardt et al. 2013) at $z = 1.48$. From spectra of 15 cluster member galaxies, Bayliss et al. (2014) found an elevated occurrence of star formation in the galaxies of this cluster. All 15 members had SFRs $\geq$1.5 M$_\odot$ yr^{-1}. The *HST* image of this cluster, along with the positions of the transients discovered during See Change are also shown in Fig. 2.

The *Spitzer* Adaptation of the Red-sequence Cluster Survey (SpARCS) was a z'-band imaging programme of the SWIRE *Spitzer* fields (which have been observed with all seven *Spitzer* passbands). It used the $z - 3.6\,\mu$m colour to find candidate clusters (by flagging large overdensities in a narrow colour range; see e.g. Wilson et al. 2009; Muzzin et al. 2009). The stellar bump sequence method was also used to discover clusters (e.g. Muzzin et al. 2013). Three clusters discovered in the SpARCS survey were monitored by See Change: SpARCS J022427–032354 (hereafter SpARCS0224) at $z = 1.63$, SpARCS J033056–284300 (hereafter SpARCS0330) at $z = 1.63$ and SpARCS J003550–431224 (hereafter SpARCS0035) at $z = 1.34$ (Lidman et al. 2012).

XDCP J0044.0-2033 (hereafter XDCP0044) is an X-ray luminous massive cluster at $z = 1.58$ (Santos et al. 2011). The cluster shows a reversal of the star formation density relation, where the SFR in the projected cluster core is four times higher than in the outskirts (Santos et al. 2015). See also Fassbender et al. (2014) for detailed observations of XDCP0044. MOO J1014+0038 (hereafter MOO1014) was found by the Massive and Distant Clusters of WISE Survey (Brodwin et al. 2015) and is at a redshift of $z = 1.231$ (Decker et al. 2019).

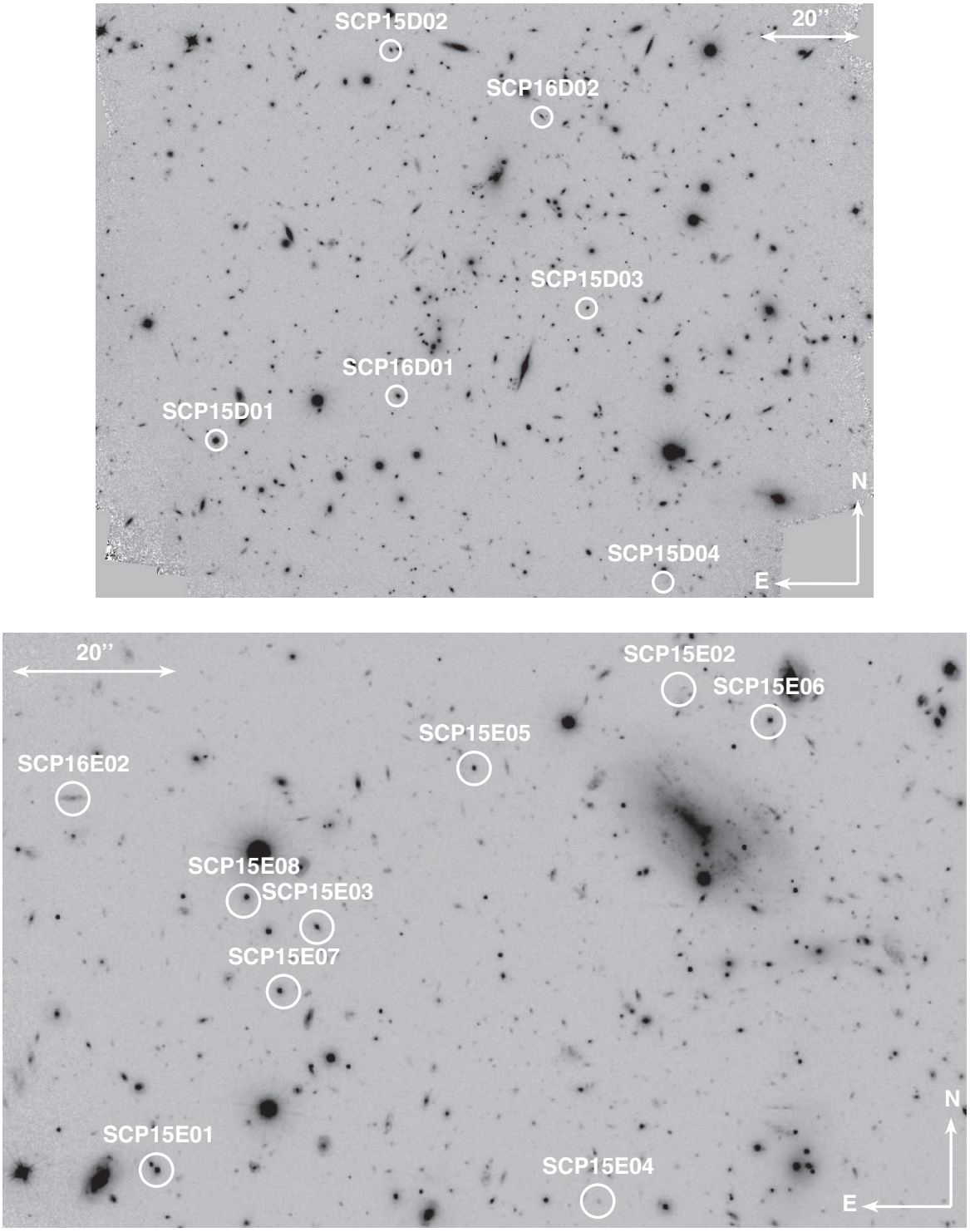

Figure 2. Stacked *HST* WFC3/IR *F*105*W* See Change image of clusters SPT2106 (top panel) and SPT2040 (bottom panel), with the positions of all transients discovered through the See Change programme indicated. A square-root flux scale is used to aid the visualization of the faint objects.

3 IDENTIFICATION OF TRANSIENTS

The See Change programme observed these $z > 1.1$ clusters with *HST*, using a five-week cadence, for one orbit split between WFC3/UVIS *F*814*W*, and the WFC3/IR *F*105*W* and *F*140*W* filters at each epoch. Additional target of opportunity (ToO) *HST* orbits were assigned to clusters with live SNe to ensure high-signal-to-noise ratio (S/N) observations in at least three bands, allowing the applied colour standardization to be tested, as well as increasing the sampling of the light curve. The 50 per cent completeness for a simulated SN detection was AB mag 26.6 in *F*105*W* + filters (Hayden et al., in preparation). The transients were discovered by subtracting *HST* reference images (built up as part of this survey)

Table 1. The letter used in the naming of each transient discovered in the field of a given cluster.

Cluster	Redshift	SN Designation
SPT0205	1.32	A
MOO1014	1.23	C
SPT2106	1.13	D
SPT2040	1.48	E
SpARCS0035	1.34	F
XDCP0044	1.58	G
SpARCS0330	1.63	H
SpARCS0224	1.63	I

from the most recent image, and then performing photometry on any excess flux that was consistent with the expected PSF of a point-source

The highest priority targets for the ground-based spectroscopic programmes were candidate $z > 1$ SNe Ia. For the purpose of triggering spectroscopic follow-up, an object was determined to be a potential SN Ia if the magnitude and colours of the transient were consistent with an SN Ia and the photometric redshift of the host galaxy gave the possibility that it was at $z > 1$. At the point of obtaining spectroscopy, we therefore did not have to be confident that a given transient was a $z > 1$ SN Ia, just that there was a reasonable possibility that it was.

The See Change naming system indicates the sequential order of the transients discovered in the field of a given cluster in a given year, where each cluster has an associated letter, summarized in Table 1. For example, SCP16A04 was the fourth transient to be discovered in the field of SPT0205 during the year 2016.

Due to the lack of live SN spectra, See Change relies on the photometric classification of each transient. The photometric typing employed for the See Change survey combines the light-curve classification procedure discussed in detail by Rubin et al. (2018), the redshift information, and a single-epoch typing. This single-epoch typing will be presented by Hayden et al. (in preparation) and is based on comparing the observed flux in each *HST* filter, when the SN is near peak brightness, to Monte Carlo simulations of different SN types at different redshifts. This single-epoch typing yields a type probability at any given redshift (in the range $0.5 \leq z \leq 2.0$), which can be combined with the spectroscopic redshift to give a classification. The light-curve classifier fits the photometry with various templates of different SN types, both light-curve shape in a band, and the colour. A sample of SN Ia templates was constructed from SALT2 (Guy et al. 2007; Mosher et al. 2014), to which CC templates from SNANA (Kessler et al. 2009) and SN Ia subtypes were added. The flux in each *HST* band was then compared to the templates in a Monte Carlo simulation.

A transient is classified as an SN Ia if its probability of being an SN Ia, $\mathrm{P(Ia)} \geq 0.9$. A likely SN Ia has $0.75 \leq \mathrm{P(Ia)} < 0.9$, with a possible SN Ia having $0.25 \leq \mathrm{P(Ia)} < 0.7$ and non-SN Ia $\mathrm{P(Ia)} < 0.25$. These classifications use all available photometry and redshift information (including the spectra presented here), and are thus different from the initial classifications of a transients as candidate SN Ia when deciding on follow-up observations.

4 SPECTROSCOPIC OBSERVATIONS

The VLT data were obtained through programmes 294.A-5025, 095.A-0830, 096.A-0926, 097.A-0442, and 0100.A-0851. We used X-Shooter (Vernet et al. 2011) and the MOS mode of the FOcal Reducer/low-dispersion Spectrograph 2 (FORS2; Appenzeller et al. 1998). If suitable, FORS2 was generally preferred over X-Shooter, due to the MOS giving us the capability to obtain spectra of multiple host galaxies simultaneously, and therefore being much more time-efficient. The objects that were deemed to potentially be $z > 1$ SNe Ia were the highest priority for VLT spectroscopy. These were the only targets observed with X-Shooter, and had priority over other objects when assigning the FORS2 slit positions. Non-SN Ia See Change transients were the second priority when assigning the FORS2 slits. The VLT observations of See Change transient host galaxies are summarized in Table A1. The average brightness of our target SN Ia host galaxies was $F814W = 23.7$ mag (AB), ranging from the brightest SCP15D01 at $F814W = 21.4$ mag to SCP15A01 at mag ∼28.

4.1 FORS2

The positions of the FORS2 slitlets were assigned using the FORS Instrumental Mask Simulator (`FIMS`). The FoV of the *HST* WFC3/IR channel is 123×136 arcsec^2 and we targeted the centre of each cluster with a single *HST* field repeatedly. The FoV of the FORS2 MOS is approximately 6.8×6.8 arcmin^2, so the host galaxies of the See Change transients never filled all 19 slitlets on the MOS. Therefore, if possible we placed remaining slitlets on cluster–galaxy candidates. Typically, the bluest feature we targeted for redshift determination was [O II] 3727 Å, which at $z = 1.5$ is at an observed wavelength of 9318 Å. The optical FORS2 spectroscopy is therefore only realistically feasible for the $z < 1.5$ targets. At the lower redshift end of our SN Ia target sample, $z = 1$, the line is at 7454 Å. We therefore selected the GRIS_300I+11 grism, which gives a wavelength coverage of 6000–11000 Å and a resolution of $R = 660$ at the central wavelength of 8600 Å. We used a slit width of 1 arcsec and split each observation into two exposures, with a small spatial offset applied, typically ∼3 arcsec. While our top priority targets when observing with FORS2 were always the See Change candidates deemed likely to be high-redshift SNe Ia, all See Change transients discovered in any of the clusters targeted with FORS2 were observed at least once. As will be described below, we were able to obtain secure redshifts for the majority of both the SNe Ia and non-SNe Ia that we targeted with FORS2.

4.2 X-Shooter

The X-Shooter time was split between ToO and non-ToO observations. The non-ToO observations were primarily focused on obtaining redshifts of the host galaxies of SN Ia candidates that were likely at $z > 1.4$, meaning the [O II] 3727 Å and Ca II H & K lines start to become redshifted too far out of the optical, making a redshift difficult to obtain from FORS2 data. The ToO time was primarily used when a redshift was vital for deciding whether to trigger *HST* ToO orbits on a particular candidate, and therefore obtaining a redshift was time-critical. Our X-Shooter observing strategy was optimized for the near-infrared (NIR) observations. The total integration time in the NIR-arm of each observation block (OB) was 1 h (this was split into several individual exposures), with the UVB and VIS-arms exposures then set at the maximum possible without adding to the total observation time (typically ∼0.758 and ∼0.872 h, respectively). To aid the NIR sky-subtraction, we employed nodding and a 1 arcsec dither. The spatial distance of the nodding was sometimes restricted by the presence of other sources that would be on the slit at the requested position angle, and was therefore set on a case-by-case basis. Slits widths of 1.0,

0.9, and 0.9 arcsec were used in the UVB, VIS, and NIR arms, respectively.

5 DATA REDUCTION

5.1 FORS2 spectra

The FORS2 spectra were bias corrected, flat fielded and wavelength calibrated using the `ESOReflex` pipeline (Freudling et al. 2013). As each OB consisted of two exposures with a spatial offset, the sky subtraction is performed by subtracting one exposure from the other, thus sampling the same background as the traces in the two positions along the slit. This sky-subtraction method will generally reduce the S/N by $\sqrt{2}$. However, we found that the systematics associated with the sky-subtraction were significantly reduced. Given that the majority of the features, we were trying to detect were at observed wavelengths of >8000 Å, where for spectroscopy of such faint sources there are many sky lines, we therefore determined that on balance utilizing the offsets was the better method for recovering reliable redshifts for these faint host galaxies.

5.1.1 Extraction of 1D *spectra*

The path of the trace was defined using a low-order polynomial fit in the `aptrace` algorithm in `IRAF`[1] (Tody 1986). The traces were fit by a Gaussian in the spatial direction (after binning in wavelength due to the low S/N per pixel). As we were observing extended sources, the width of the traces would be influenced by both the dimensions of the target and the atmospheric seeing. Therefore, the full width at half-maximum (FWHM) of the traces was measured independently for each object. The extracted pixels were then optimally combined using the methodology outlined by Horne (1986), where each spatial pixel at a given wavelength is assigned a weight according to its position compared to the centre of the trace and the width of the trace itself. Each pair of 1D spectra were then summed. This completes the sky subtraction by removing sky variations that are dependent on the position along the slit. We find that this produces a good sky subtraction, with relatively little systematic error associated with the sky lines.

5.1.2 Flux calibration

Flux calibration was performed using the ESO standards and calculated using data products from the `ESOReflex` pipeline. This was then applied to each optimally combined 1D spectrum. The individual flux-calibrated 1D spectra of each host galaxy were then stacked using a weighted mean to produce the final spectra presented here.

5.1.3 Error spectra

The error spectra of the wavelength-calibrated 2d spectra were obtained from the `ESOReflex` pipeline. The errors were then propagated through the extraction, combining, and flux calibration process described above. These final spectra, with accurate errors, allowed us to compute realistic uncertainties on the emission-line fluxes. This was particularly important for the apparently passive galaxies, as the errors were used to compute the upper limits on the emission lines. The error spectra were also used in the cross-correlation analysis (see Section 6).

5.2 X-Shooter spectra

The X-Shooter data were reduced to 2D, wavelength-calibrated, sky-subtracted, flux-calibrated spectra using the `ESOReflex` pipeline. The utilization of the nod and dither gave a very good sky subtraction. The extraction and optimal combining were then performed using a modified (due to the differing sky-subtraction method and resolution) version of the FORS2 reduction described in Section 5.1.

5.3 Telluric correction

We corrected the spectra for telluric absorption using `Molecfit` (Kausch et al. 2015; Smette et al. 2015). The choice of spectrum used for the telluric fitting was made on a case-by-case basis for the FORS2 data. Continuum fitting was required, which can prove problematic if the S/N is particularly poor, exacerbated in some cases by emission or absorption lines being coincident with regions near telluric absorption. Due to this, the final combined spectrum was only used to determine the telluric correction for the higher S/N cases. In the majority of cases, the brightest object that appears in any of the slits of a single MOS observation was extracted and the atmospheric absorption fitted to that. The resulting telluric correction was then applied to the (fainter) objects in the other slits. The individual telluric-corrected spectra of a particular object were then combined as outlined in Section 5.1.

The X-Shooter data were corrected for atmospheric absorption using standard stars observed shortly after or before the science observation, and at a similar airmass. The 1D spectrum of each standard star observation was extracted using the `ESOReflex` pipeline. We then used `Molecfit` to correct the standard observation for atmospheric absorption due to H_2O, O_2, CO_2, CO, and CH_4. This correction was then applied to the corresponding science observation. Each corrected science observation was then combined as outlined above to produce a single spectrum for each object.

5.4 Host galaxy photometry and absolute flux calibration

One of the aims of this work was to obtain good constraints on the stellar mass of each SN Ia host galaxy, which required absolute flux calibration of our spectra (see Section 7 for details on how we determined the host galaxy parameters). For any galaxy that hosted an SN Ia, likely SN Ia or possible SN Ia, we used the *HST* photometry and filter responses – namely the *F*814*W*, *F*140*W*, and *F*160*W* filters – to make an absolute flux calibration. The *HST* photometry was performed using `LAMBDAR` (Wright et al. 2016). Photometric apertures were defined using `SEP`[2] (Bertin & Arnouts 1996; Barbary 2016). We detected objects greater than 2σ above background, and determined their apertures using the Kron radius method, with a radius argument of 5 and an ellipse scaling factor of 2.5 (see `SEP` documentation for aperture photometry equivalent to FLUX_AUTO in `Source Extractor`). Each aperture within 7 arcsec of an SN was reviewed manually, and resized if the Kron radius was artificially enlarged by a nearby object. Possible contaminant galaxies overlapping the main apertures were added if they blended

[1] `IRAF` is distributed by the National Optical Astronomy Observatory, which is operated by the Association of Universities for Research in Astronomy (AURA) under a cooperative agreement with the National Science Foundation.

[2] https://sep.readthedocs.io/en/v1.0.x/

Table 2. *HST* photometry of galaxies that hosted an SN Ia, likely SN Ia or possible SN Ia, and for which we were able to obtain a spectroscopic redshift in this work. This photometry was used in the SED fitting.

Transient Name	Host galaxy photometry (μJ)					
	*F*606*W*	*F*814*W*	*F*105*W*	*F*125*W*	*F*140*W*	*F*160*W*
SCP15A03	–	1.00 ± 0.09	3.68 ± 0.02	–	6.24 ± 0.02	7.38 ± 0.03
SCP15A04	1.87 ± 0.14	3.93 ± 0.34	11.79 ± 0.19	–	16.85 ± 0.26	19.46 ± 0.40
SCP15A05	1.55 ± 0.19	3.58 ± 0.38	10.65 ± 0.11	–	14.18 ± 0.24	15.59 ± 0.18
SCP15A06	–	2.37 ± 0.17	10.07 ± 0.13	–	19.89 ± 0.29	23.72 ± 0.26
SCP15C01	–	1.37 ± 0.14	2.15 ± 0.04	–	2.81 ± 0.06	–
SCP15C03	–	1.09 ± 0.50	3.09 ± 1.15	4.59 ± 1.40	5.64 ± 1.63	6.96 ± 2.04
SCP15C04	–	1.50 ± 0.05	3.72 ± 0.02	4.87 ± 0.03	5.94 ± 0.03	6.86 ± 0.04
SCP15D01	–	9.96 ± 0.24	13.22 ± 0.24	–	14.75 ± 0.25	–
SCP15D02	0.92 ± 0.05	2.17 ± 0.14	3.61 ± 0.07	–	5.64 ± 0.11	–
SCP15D03	–	1.25 ± 0.14	2.90 ± 0.05	–	3.93 ± 0.04	–
SCP16D01	–	2.09 ± 0.12	7.20 ± 0.07	–	12.25 ± 0.14	–
SCP15E06	0.38 ± 0.22	0.79 ± 0.25	4.12 ± 0.26	–	8.21 ± 0.16	10.01 ± 0.25
SCP15E07	0.28 ± 0.08	1.18 ± 0.10	5.44 ± 0.07	–	11.43 ± 0.11	13.96 ± 0.15
SCP15E08	3.98 ± 0.12	7.98 ± 0.17	12.28 ± 0.19	–	16.81 ± 0.19	18.67 ± 0.31
SCP15G01	–	1.21 ± 0.39	4.57 ± 0.22	–	10.65 ± 0.36	13.63 ± 0.37

with the likely SN host. The units of the *HST* stacked images were changed from electrons per second to electrons using the median exposure time of pixels in the drizzled image, so that LAMBDAR could accurately model the counting statistics of each pixel. The aperture was defined for the *F*105*W* stacked image, and the same aperture was then used in every available *HST* filter. In addition to using the *HST* photometry to perform an absolute flux calibration of our spectra, we also use it in the analysis when determining galaxy parameters. For this, we use all available *HST* photometry: *F*606*W*, *F*814*W*, *F*105*W*, *F*125*W*, *F*140*W* and *F*160*W* filters. All of our SN Ia host galaxy *HST* photometry is shown in Table 2.

We assume that the galaxy light sampled in our spectra is representative of the overall galaxy light. It is possible this is not always the case. For example, in an edge-on spiral, it is possible that if the slit was placed parallel with the disc a larger emission-line flux would be derived than if the slit were placed through the centre of the galaxy, perpendicular to the disc (thus sampling a lower proportion of the disc light). However, given our targets generally have a small angular size, which is convolved with the seeing, in most cases, the assumption should be reasonable and we therefore assume this to be the case when deriving SFRs from emission-line fluxes.

6 REDSHIFT DETERMINATION

Obtaining redshifts from passive galaxies can be difficult with low S/N spectra. This can be made even more difficult if, for example, the position of the Ca II H & K lines are in a low S/N region, either due to the throughput of the spectrograph, detector sensitivity, or atmospheric absorption or sky lines. We therefore employed a weighted cross-correlation to help derive secure redshifts, cross-correlating our spectra with the galaxy spectral cross-correlation templates from SDSS DR5 (Adelman-McCarthy et al. 2007).[3] The weighted cross-correlation allows for the exclusion of bad data, with the remaining data then weighted by the inverse of the variance (Kelson, Martini & Mulchaey 2003). As our data are in the red/NIR, this is particularly useful as certain wavelength pixels will have significantly lower S/N than neighbouring pixels, due to sky lines and telluric features.

For the majority of objects where it was possible to derive a redshift with high confidence from the cross-correlation, we found that the features were already visible by visual inspection. This could be in part due to the relatively limited rest-frame wavelength coverage of the FORS2 data. The one example where this is not the case is SCP15E07 (with both FORS2 and X-Shooter data), which we therefore show as an example of the cross-correlation output in Fig. 3. The figure also illustrates the *HST* photometry of the SCP15E07 host, and synthetic photometry of the best-fitting SED in the same filters.

We compare all of our spectroscopic redshifts for the See Change host galaxies to the respective photometric redshifts in Fig. 4. Following Hildebrandt et al. (2010), we use the definition of a galaxy being a photometric redshift outlier if:

$$\frac{|z_{\rm phot} - z_{\rm spec}|}{(1 + z_{\rm spec})} > 0.15.$$

The host galaxy of SCP15E08 (at $z_{\rm spec} = 2.02$) is the only clear outlier. It is worth noting, however, that the light from this host galaxy is presumably dominated by the AGN at its core. We note that the relationship between the photometric redshifts and our spectroscopic redshifts appears 'flatter' than the ideal scenario of $z_{\rm phot} = z_{\rm spec}$.

7 GALAXY PARAMETERS

The majority of our spectra are taken using FORS2, with a wavelength coverage of around 0.61–1 μm (the sensitivity drops off dramatically at >1 μm). This, combined with the high redshifts of our targets, means that measurement of SFRs from Hα (or Hβ) is typically not possible, as the line is redshifted out of the observed wavelength range, and we have to rely on the [O II] doublet at 3727 Å for our (emission-line) cluster galaxy SFR constraints. Any further mention of [O II] in this paper refers to this 3727 Å doublet. The SFRs derived from [O II] can vary significantly from those derived from Hα, due in large part to reddening and metallicity (Kewley, Geller & Jansen 2004). At low SFRs the [O II] emission from a galaxy can be contaminated by post-AGB stars (Belfiore et al. 2016). For these reasons, in addition to it being subject to less extinction,

[3] http://classic.sdss.org/dr5/algorithms/spectemplates/index.html

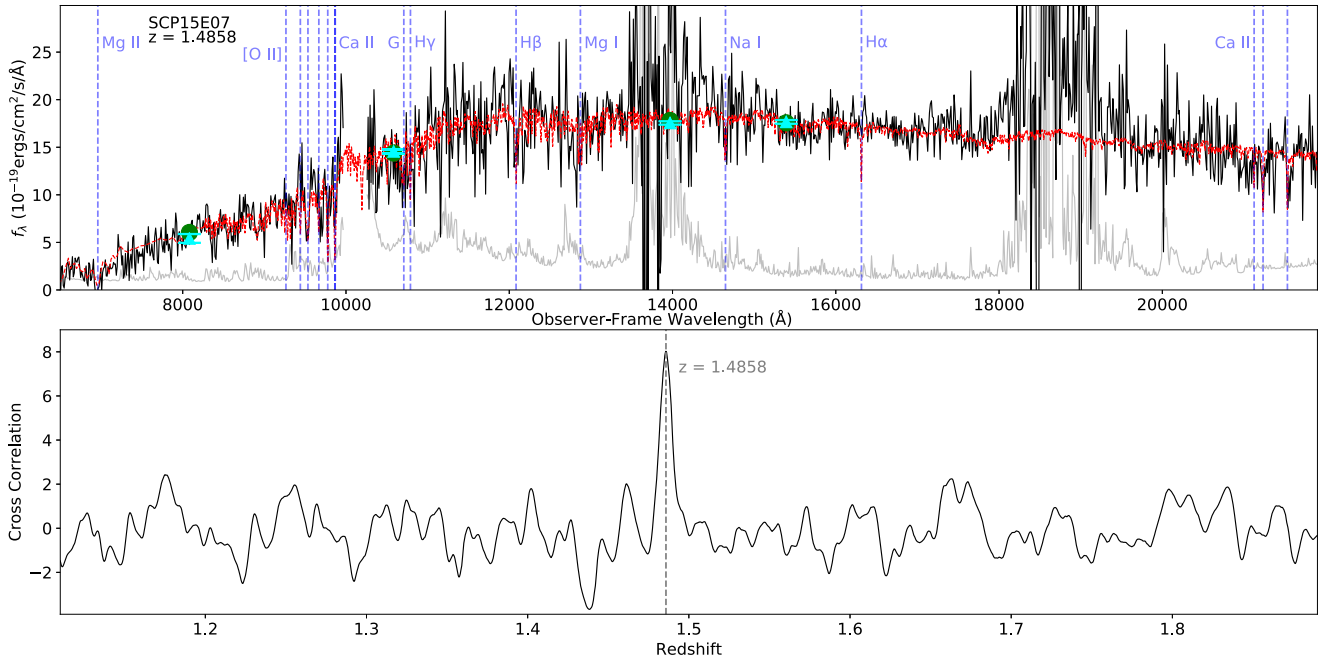

Figure 3. Upper panel: combined FORS2 and X-Shooter spectrum of the host galaxy of SN Ia SCP15E07. The binned VLT data is the solid black line, with the best-fitting FAST SED shown by the dashed red line. The solid grey line shows the errors on the spectrum. Common lines seen in galaxy spectra are also indicated. The green-filled circles show synthetic photometry of the best-fitting FAST SED, using the *HST* filters, with the cyan triangular points showing the actual *HST* photometry of the host galaxies (in the same filters). Lower panel: the only significant peak shown in the cross-correlation is centred at $z = 1.4858$, with $\hat{r} > 5$. The telluric correction was generally good, however, in this particular case there appears some overcorrection in the H_2O feature between ∼1.82 and 1.92 μm. As noted in the text, regions of high atmospheric absorption are de-weighted in the cross-correlation. The NIR regions of very high atmospheric absorption (i.e. between ∼1.35–1.42 μm, and between ∼1.82 and 1.92 μm) are excluded from the FAST fitting of the stellar population, so systematic errors in the correction here will not affect galaxy parameters derived by FAST.

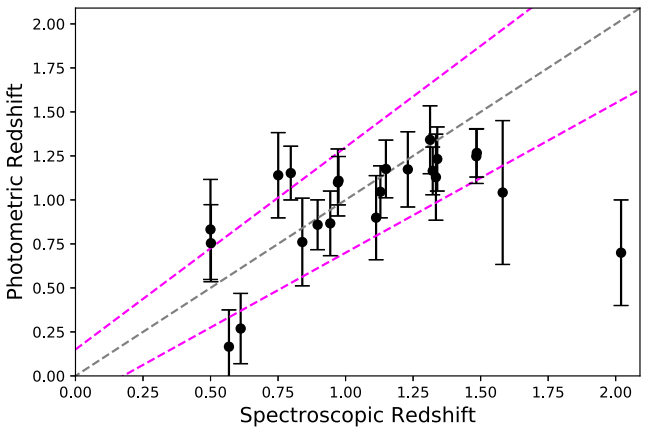

Figure 4. Comparison between the photometric redshifts for the See Change host galaxies (both SN Ia and non-Ia) and the spectroscopic redshifts derived from our spectra. The grey-dashed line indicates $z_{\rm phot} = z_{\rm spec}$. A photometric redshift lying outside of the area encompassed by the two magenta-dashed lines is considered an outlier, as defined in Section 6. The outlier at $z = 2.02$ is the host of SN Ia SCP15E08. The light from this galaxy is likely dominated by the AGN at its centre.

we use Hα to estimate the SFR where we have a spectrum that includes both Hα and [O II]. For the SN Ia host galaxies presented in this work, Hα is always in the NIR, so it is only possible to use this line if we have an X-Shooter spectrum. For those where only [O II] constraints are available, we assume all of the emission is associated with star formation and there is no contamination. Another potential source of emission-line contamination is active galactic nuclei (AGNs). Galaxies, where the emission lines are dominated by the contribution from AGN, are usually differentiated from those where the emission lines mainly arise from star formation using emission-line ratios (e.g. [N II]/Hα and [O III]/Hβ). However, these regions are typically not covered by our spectra, with only the [O II] line well covered, so they cannot be conclusively filtered out.

The FAST (Kriek et al. 2009) code fits stellar population synthesis templates to both spectra and photometry. The code gives best-fitting galaxy parameters, such as stellar age, stellar mass, extinction, and SFR, with the errors on the derived parameters from Monte Carlo simulations. We utilized FAST, with the filters from EAZY (Brammer, van Dokkum & Coppi 2008), on our SN Ia host galaxy data. The use of FAST allowed us to simultaneously fit the *HST* photometry presented in Table 2 and the calibrated ground-based spectra to constrain the stellar mass, SFR, internal extinction, and stellar age of each galaxy. The inclusion of the spectra in the fitting tightens the constraints significantly, by breaking the degeneracy between reddening and age that arises from only fitting photometry. In some cases, the uncertainties on the derived parameters are significantly influenced by the uncertainties on the *HST* photometry, which can be relatively high in the *F*814W band.

As FAST fits only the stellar population of a galaxy (and thus does not consider emission lines), we use the best-fitting FAST SED of each galaxy as the continuum from which to measure any emission. Before the measurement is made, we normalize the flux of the FAST SED to the data in the region around the line of interest (but excluding the line itself). As FAST fits the entire spectrum and

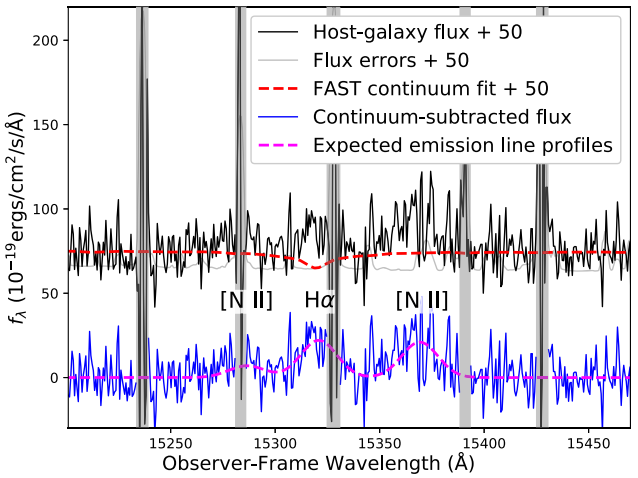

Figure 5. Unbinned continuum-subtracted X-Shooter spectrum of the region around Hα for the SCP15A04 and SCP16A04 host galaxy. The galaxy flux, errors, and continuum fit are offset above. For visualization, the expected (i.e. fixed [N II] 6548/6583 Å ratio, etc.) emission-line profiles of Hα, along with [N II] 6548 and 6583 Å are shown in magenta. When calculating the emission-line fluxes in the X-Shooter data, regions affected by sky lines (indicated by the shaded grey regions) are not included in the measurement.

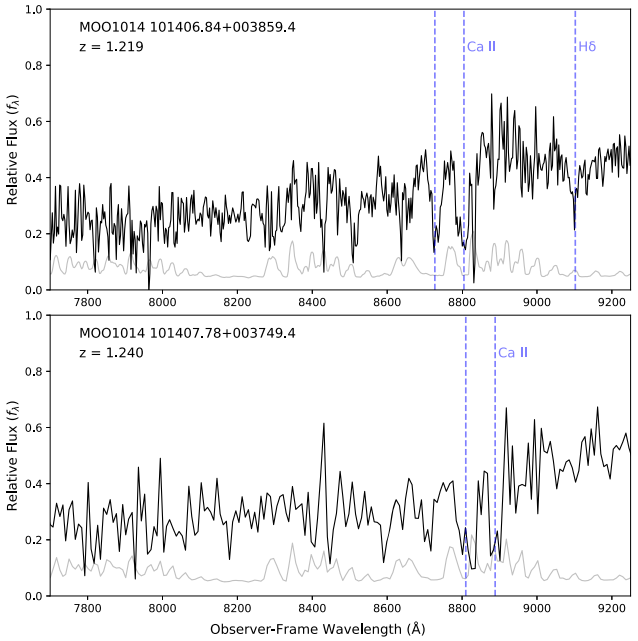

Figure 6. Spectra of two galaxies in the field of cluster MOO1014 that did not host a transient during the See Change survey. These both show Ca II H & K absorption, enabling us to derive redshifts. The spectra are represented by black lines, with the grey lines showing the associated error spectra. The wavelengths of selected absorption lines are indicated.

photometry, we do this in order to remove any systematic offset that may arise in specific regions of the spectrum from the fitting. If no emission line is obvious, we force an emission-line measurement assuming a Gaussian with FWHM $= 200 \pm 100$ km s^{-1}, which is convolved with the resolution of the spectra. The difference (positive or negative) in the spectrum flux from the FAST SED is then extracted using a weighted Gaussian. The uncertainty in the emission-line measurement is then derived from a propagation of the errors on the spectra and the uncertainty in the *HST* photometry used in the absolute flux calibration. Using the FAST SED in this way to aid in the emission-line measurements has two advantages: (1) our spectra have relatively low S/N, so determining the continuum level in a small region near a given emission line can be difficult, and (2) it effectively corrects for stellar absorption, which is particularly important in our measurements of Hα and Hβ emission. An example of an emission-line measurement is shown in Fig. 5. In the case of the (higher resolution) X-Shooter spectra, where the sky lines are narrow, the wavelengths that are badly affected by sky lines are masked from the emission-line measurements. In such cases, the excess flux is extracted using a weighted Gaussian with those wavelengths excluded, with the total flux and errors then propagated through to account for the absent wavelength pixels.

The emission-line measurements are converted into luminosities assuming a flat cosmology with $H_0 = 70$ km s^{-1} Mpc^{-1} and $\Omega_M = 0.3$. They are corrected for foreground Galactic extinction using extinction map values from Schlafly & Finkbeiner 2011. To convert the emission-line luminosities into SFRs, we must also correct for host-galaxy extinction. The host-galaxy extinction constraints derived by FAST are for the stellar population. On average, the stellar population of a galaxy will be subject to lower dust extinction than the emission lines. In order to derive SFRs from our emission lines, we use $E(B-V)_{\rm stellar} = 0.44 \times E(B-V)_{\rm nebular}$ from Calzetti et al. (2000). We assume a Cardelli, Clayton & Mathis (1989) reddening law with $R_V = 3.1$ for both foreground and host galaxy extinction. These resulting dust-corrected line luminosities are then converted to SFRs using SFR $= 5.45 \times 10^{-42}\, L$(H$\alpha$) (M$_\odot$ yr^{-1})/(erg s^{-1}) from Calzetti et al. (2010) and SFR $= 2.65 \times 10^{-41}\, L$([O II]) (M$_\odot$ yr^{-1})/(erg s^{-1}) from Meyers et al. (2012). We also use Hβ to determine SFR by assuming Case B recombination (i.e. L(Hα)/L(Hβ)=2.86 at 10^4 K) and the Calzetti et al. (2010) Hα relationship, resulting in SFR $= 1.56 \times 10^{-41}\, L$(H$\beta$) (M$_\odot$ yr^{-1})/(erg s^{-1}). We caution here that these derived SFRs assume no emission-line contamination (see discussion above).

8 RESULTS

Here, we present the See Change host-galaxy spectra and derived parameters. The host structure and where each SN resides with respect to the host can be seen in Appendix B.

8.1 The spectroscopic redshift of MOO1014

At the beginning of the See Change survey, MOO1014 had a photometric redshift of 1.27 ± 0.08 (Brodwin et al. 2015), but no published spectroscopic redshift. We therefore used the spectra of galaxies observed with FORS2 to estimate the redshift of the cluster. Our spectra of two galaxies that did not host a See Change transient are displayed in Fig. 6 and have redshifts of $z = 1.219$ and 1.240. Additionally, the host galaxy of SN Ia SCP15C04 is at $z = 1.232$ (see Section 8.3.7 for further details on that host). These three galaxies are at an average redshift of $z = 1.230$, essentially identical with the MOO1014 redshift of $z = 1.231$ published by Decker et al. (2019).

8.2 Host galaxies of See Change transients that are not SNe Ia

The redshift of each host galaxy of a See Change transient that is not believed to be an SN Ia is summarized in Table 3. The conclusion

Table 3. Details of host galaxy spectra of See Change transients that are classified as non-SNe Ia.

SCP Transient	Redshift	Host features identified
SCP15A02	0.8966	[O II] 3727 Å, Ca II H & K
SCP15A07	0.5015	Hα (photo-z constrains to $z < 1$, implying single emission line is Hα)
SCP16A01	0.4998	Hβ, [O III] 4959 & 5007 Å, Hα
SCP16A02	0.7971	[O II] 3727 Å, Ca II H & K, Hβ
SCP16A03	1.335?	[O II] 3727 Å? (Single strong emission line, alternatively Hα at $z = 0.326$)
SCP15C02	0.7506	[O II] 3727 Å, Ca II H & K, Hβ
SCP15C03	–	Emission line at ∼7490 Å possibly [O II] 3727 Å
SCP16C01	0.9739	[O II], Hϵ, Hδ, Hγ, Hβ, [O III] 4959 and 5007 Å
SCP16C02	–	None
SCP16D02	–	None
SCP16D03	0.6118	[Ne III] 3869 Å, Hδ, Hγ, Hβ, [O III] 4959 and 5007 Å
SCP15E01	0.8398	[O II] 3727 Å, [Ne III] 3869 Å, Hγ, Hβ, [O III] 4959 and 5007 Å
SCP15E02	–	None
SCP15E05	–	None
SCP16E02	0.9435	[O II] 3727 Å, [O III] 4959 & 5007 Å

that these are not likely to be SNe Ia is based on all of the available data, including the host spectroscopy itself, which in some cases directly helped break degeneracies in the photometric classification. The photometric classification of each See Change transient will be presented in Hayden et al. (in preparation). The individual spectra of galaxies that hosted non-SN Ia transients during the See Change survey are shown in Fig. 7. Below, we discuss specific cases where either the transient is worth noting, or the redshift determination requires further explanation.

The host galaxy of SCP15A07 has a single strong emission line, consistent with Hα at $z = 0.5015$. The line would also be consistent with [O II] at $z = 1.644$, but the photometric redshift strongly favours the lower redshift. The host galaxy of SCP16A03 shows a very strong emission line at 8705 Å. If this strong emission line is [O II] 3727 Å, the galaxy is at $z = 1.335$ and in the SPT0205 cluster. However, if the transient is in the cluster, it is too bright in the F814W *HST* observations (which would be rest-frame *U*-band) to be a normal SN Ia, so may be a luminous SN II. Alternatively, the line may be Hα at $z = 0.326$. As can be seen in Fig. B1, there is another galaxy very close to the host of SCP15C03, with the spiral arm extending to overlap the SN host galaxy. The emission line at ∼7490 Å could be associated with the spiral arm of this other galaxy and not the SN host. It is worth noting that at the cluster redshift of $z = 1.23$, a 4000 Å break would be at ∼8900 Å. It can be seen from Fig. 7 that there appears higher continuum flux redwards of 8900 Å compared to bluer wavelengths. From the data in hand though, it is not possible to conclusively confirm the redshift of the SCP15C03 host galaxy, hence we do not report a redshift in Table 3.

8.3 See change SN Ia hosts

The host redshifts of each SN Ia found during the See Change survey, and emission-line measurements, are summarized in Table 4. The individual galaxy spectra are presented and discussed below. Note that emission-line fluxes quoted in this section are as measured, and not corrected for extinction. However, any line ratios or SFR constraints have been corrected for extinction, as outlined in Section 7.

8.3.1 SCP15A03

The host galaxy of SN Ia SCP15A03 was identified to be at $z = 1.3395$, with the spectrum showing Ca II H & K and H9/CN absorption lines. The host spectrum, which is shown in Fig. 8, shows weak evidence of [O II] emission. Assuming this emission is associated with star formation, and not contaminated by other sources, implies a SFR of 12^{+7}_{-10}, $M_\odot\,yr^{-1}$, whereas the FAST SED fitting finds an SFR of $0.0^{+0.3}_{0.0}$, $M_\odot\,yr^{-1}$. Given the large uncertainties in the emission-line SFR measurement, this represents only an $\sim 1\sigma$ disagreement. Using FAST, we derive a stellar age of $1.0^{+0.1}_{-0.3}$ Gyr for this host galaxy.

8.3.2 SCP15A04 and SCP16A04

During the See Change survey, one galaxy in SPT0205 produced two individual SNe Ia, SCP15A04 and SCP16A04. The galaxy shows [O II] emission in the optical (seen in both the FORS2 and X-Shooter spectra), along with Ca II H & K at $z = 1.3345$. The X-Shooter NIR spectrum reveals emission lines from Hα, and [N II] 6548 and 6583 Å. The measurement of these emission-line fluxes is illustrated in Fig. 5, and we find $\log([\mathrm{N\,II}]\,\lambda6583/\mathrm{H}\alpha) = 0.03^{+0.12}_{-0.17}$, which indicates there is likely at least some AGN contribution to the emission-line flux (see e.g. Kewley et al. 2001; Kauffmann et al. 2003). Hβ and [O III] are in regions of very poor S/N, so no meaningful measurement can be made for those. If the Hα flux is associated with star formation, an SFR of $23^{+11}_{-16}\,M_\odot\,yr^{-1}$ would be implied, although given the [N II] λ6583/Hα ratio, this should be considered an upper limit. The FAST SED fitting indicates an SFR of $0.0^{+12.3}_{-0.0}\,M_\odot\,yr^{-1}$, although this assumes that any AGN activity does not contribute significantly to the continuum. FAST implies a stellar age of $0.2^{+0.5}_{-0.1}$ Gyr for this galaxy. Due to this evidence of AGN activity, we also run a modified version of FAST that includes an AGN component in the fitting (Aird, Coil & Georgakakis 2017, 2018). The results for with and without an AGN component in the fitting are summarized in Table 5 and show that in this specific case, the parameters we derive for the two cases are consistent with each other.

8.3.3 SCP15A05

The host galaxy of SCP15A05 shows Ca II H & K at $z = 1.3227$, along with several other absorption features at that redshift, including strong Balmer lines. We also detect Mg II 2800 Å absorption. The FORS2 and X-Shooter spectra of this galaxy are shown in Fig. 8. After removing the effects of a sky line in part of the expected

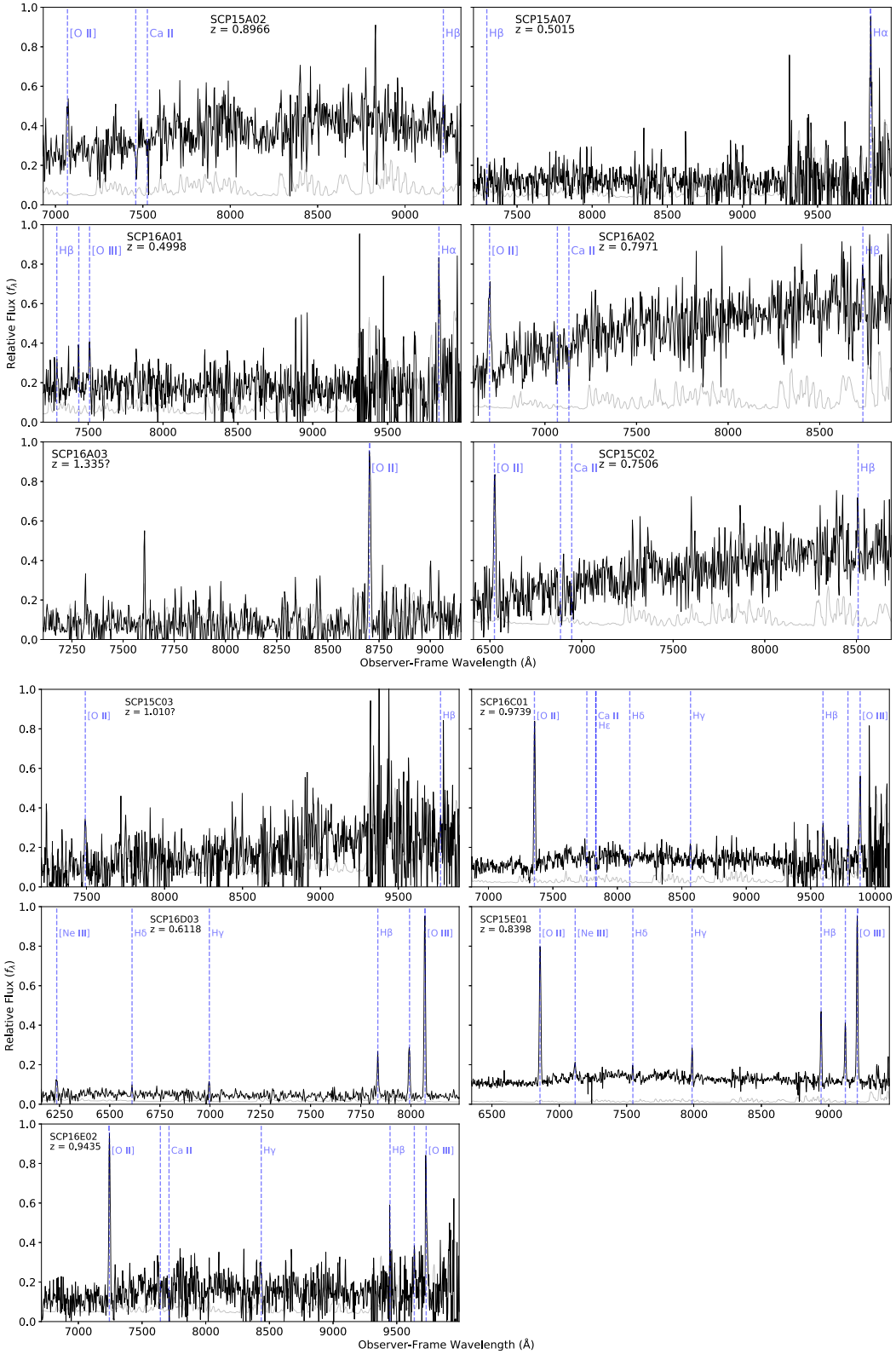

Figure 7. The FORS2 spectra of the host galaxies of non-SN Ia transients found during the See Change search. Key as in Fig. 6.

emission profile as outlined in Section 7, we measure a Hα flux of $(5.2 \pm 3.8) \times 10^{-18}$ erg s^{-1}. The Hα measurement implies an SFR of $0.7^{+0.9}_{-0.6}$ M$_\odot$ yr^{-1}, consistent with the FAST estimate of $5.1^{+0.0}_{-5.1}$ M$_\odot$ yr^{-1} from the stellar light. For this host galaxy, we derive a stellar age of $1.0^{+0.3}_{-0.8}$ Gyr. The detection of strong Balmer absorption lines indicates that A stars contribute a high fraction of the total optical light emitted by the galaxy, and thus helps to constrain the stellar age significantly.

Table 4. Redshifts and emission-line flux measurements for SN Ia, likely SN Ia and possible SN Ia host-galaxies observed by the VLT. These measurements are not corrected for reddening.

Transient	Type	Redshift	[O II] flux ($\times 10^{-18}$ erg s^{-1} cm^{-2})	Hα flux ($\times 10^{-18}$ erg s^{-1} cm^{-2})
SCP15A01	SN Ia	–	N/A	N/A
SCP15A03	SN Ia	1.3395	3.2 ± 1.2	–
SCP15A04	SN Ia	1.3345	22.9 ± 3.9	50.6 ± 10.6
SCP15A05	SN Ia	1.3227	12.1 ± 6.7	5.2 ± 3.8
SCP15A06	SN Ia	1.3128	− 0.3 ± 5.6	–
SCP16A04[a]	SN Ia	1.3345	22.9 ± 3.9	50.6 ± 10.6
SCP14C01	SN Ia	1.23	No detected host galaxy	
SCP15C01	SN Ia	0.9718	29.7 ± 3.5	–
SCP15C04	SN Ia	1.2305	− 2.1 ± 1.8	–
SCP16C03	SN Ia	2.2216	Background SN Ia[b]	
SCP15D01	SN Ia	0.5682	–	–
SCP15D02	poss Ia	1.1493	18.7 ± 2.6	–
SCP15D03	SN Ia	1.1130	4.3 ± 2.1	–
SCP15D04	SN Ia	–	N/A	N/A
SCP16D01	SN Ia	1.1289	4.2 ± 2.4	–
SCP15E03	poss Ia	–	N/A	N/A
SCP15E04	likely Ia	–	N/A	N/A
SCP15E06	SN Ia	1.484	− 0.6 ± 1.1	–
SCP15E07	SN Ia	1.4858	− 0.2 ± 1.8	5.7 ± 3.2
SCP15E08	SN Ia	2.02	Broad emission at ∼8460 Å	
SCP15G01	SN Ia	1.5817[c]	–	5.5 ± 3.8
SCP16H01	SN Ia	–	N/A	N/A
SCP15I02	poss Ia	–	N/A	N/A

[a]SCP16A04 had the same host galaxy as SCP15A04. [b]A detailed analysis of SCP16C03 is presented in Rubin et al. (2018). [c]The redshift of the SCP15G01 host galaxy is mainly from Keck data, which will be presented elsewhere, however, the Hα constraint is from our VLT data.

8.3.4 SCP15A06

The host galaxy of SCP15A06 shows strong Ca II H & K absorption lines at $z = 1.3128 \pm 0.0005$, similar to that found by Stalder et al. (2013, $z = 1.3119 \pm 0.0005$), who also derived the redshift from the Ca II lines. Our FORS2 spectrum is shown in Fig. 8. The spectrum taken by Stalder et al. (2013) can be seen in their fig. 3 (galaxy J020543.00–582936.4), which they used to derive a 3σ upper limit on the SFR of $<0.63\,M_\odot\,yr^{-1}$ from the [O II] flux, although note that this estimate does not include any correction for potential internal extinction (which we constrain to be $A_V = 0.3^{+0.6}_{-0.1}$ for the stellar light). From our FORS2 spectrum, we derive SFR $< 8.4\,M_\odot\,yr^{-1}$ from [O II] constraints and SFR $= 0.0^{+0.1}_{-0.0}\,M_\odot\,yr^{-1}$ from the FAST SED fitting. Using FAST, we derive a stellar age of $1.3^{+1.9}_{-0.3}$ Gyr for the galaxy.

8.3.5 SCP14C01

SCP14C01 was an SN discovered in our *HST* images taken 2014 December 26, with no detected host galaxy. As host galaxy spectroscopy to determine a precise redshift was not possible, we obtained live spectroscopy using director's discretionary time with FORS2 on 2015 January 20, which can be seen in Fig. 8. We find the spectrum to be consistent with an SN Ia at a redshift $z = 1.23$. This makes it one of the most distant SNe Ia with a live spectrum. Examples of higher redshift SNe Ia with live spectra include SN 2002fw at $z = 1.3$ (Riess et al. 2004), SCP06G4 at $z = 1.35$ (Morokuma et al. 2010), and the lensed SNe HFF14Tom at $z = 1.346$ (Rodney et al. 2015) and PS1-10afx at $z = 1.388$ (Chornock et al. 2013; Quimby et al. 2013). SCP14C01 is the only See Change SN Ia for which we were able to obtain a live spectrum.

Our FORS2 spectrum of SCP14C01 was analysed using the SN classification code SNID, which uses cross-correlation techniques to determine the type, age and redshift of SNe (Blondin & Tonry 2007). The results of this analysis show no confident matches. The FORS2 data were obtained between 57042.16 and 57042.27 MJD, with SCP14C01 peaking 57041.9 ± 0.8 MJD (Hayden et al., in preparation), meaning our spectra were taken when the SN was around peak brightness. When conservative peak constraints and loose redshift constraints ($0.1 \leq z \leq 2$) are placed on the SNID cross-correlation analysis, the best-matching templates are then SNe Ia in the region of $z = 1.23$. We stress, however, that these matches all have values of the parameter *r*lap < 5 when lap is constrained to $\geq$0.4, which Blondin & Tonry (2007) suggest are inconclusive. In Fig. 8, we have compared our SCP14C01 spectrum to SN Ia 2004S (Krisciunas et al. 2007) and SN Ib 1998dt (Matheson et al. 2001; Silverman et al. 2012).[4] From this analysis, it seems clear that the transient is an SN I at $z \sim 1.23$, but from the spectra alone we cannot recover a conclusive classification for the SN type. However, when including light-curve constraints, we are able to confidently classify this as an SN Ia (Hayden et al., in preparation). SCP14C01 could either be an intracluster SN Ia, or one that resides in a low-luminosity host.

8.3.6 SCP15C01

SCP15C01 was an SN Ia in the foreground of the MOO1014 cluster, with the redshift of $z = 0.9718$. This redshift was derived mainly from [O II], Hβ, and [O III] emission lines, although higher order Balmer line absorption can also be seen in the continuum (see Fig. 8). An SFR derived from the [O II] line is very poorly constrained, due in large part to the very uncertain extinction internal to the host ($A_V = 0.8^{+0.4}_{-0.8}$). For this host galaxy, we can also estimate the SFR from Hβ, which has a measured flux of $(2.16 \pm 0.30) \times 10^{-17}$ erg s^{-1}, after correcting for stellar absorption. This implies an SFR of $12^{+17}_{-10}\,M_\odot\,yr^{-1}$, which is still poorly constrained, even if better than is possible using [O II]. The FAST SED fitting indicates a low SFR of $0.2^{+2.4}_{-0.2}\,M_\odot\,yr^{-1}$, which is still consistent with the poorly constrained emission-line SFR. FAST gives a stellar age of $0.6^{+0.7}_{-0.4}$ Gyr for the host galaxy of SCP15C01.

8.3.7 SCP15C04

The FORS2 spectrum of the SCP15C04 host galaxy, which is shown in Fig. 8, shows Ca II H & K at $z = 1.2305$. The FAST analysis indicates a small amount of star formation ($2.2^{+0.9}_{-1.4}\,M_\odot\,yr^{-1}$) and a stellar age of $4.0^{+0.0}_{-1.6}$ Gyr. We do not detect [O II] emission, although the resulting 2σ limit on the SFR of $<0.9\,M_\odot\,yr^{-1}$ is still broadly consistent with that determined from the SED. The SED indicates that this galaxy has very little internal extinction, with $A_V = 0.2^{+0.1}_{-0.2}$.

8.3.8 SCP16C03

SCP16C03 was a background SN Ia at $z = 2.2216$, lensed by the MOO1014 cluster at $z = 1.23$. This redshift was derived

[4]These were retrieved via the Open Supernova Catalog; Guillochon et al. (2017); https://sne.space.

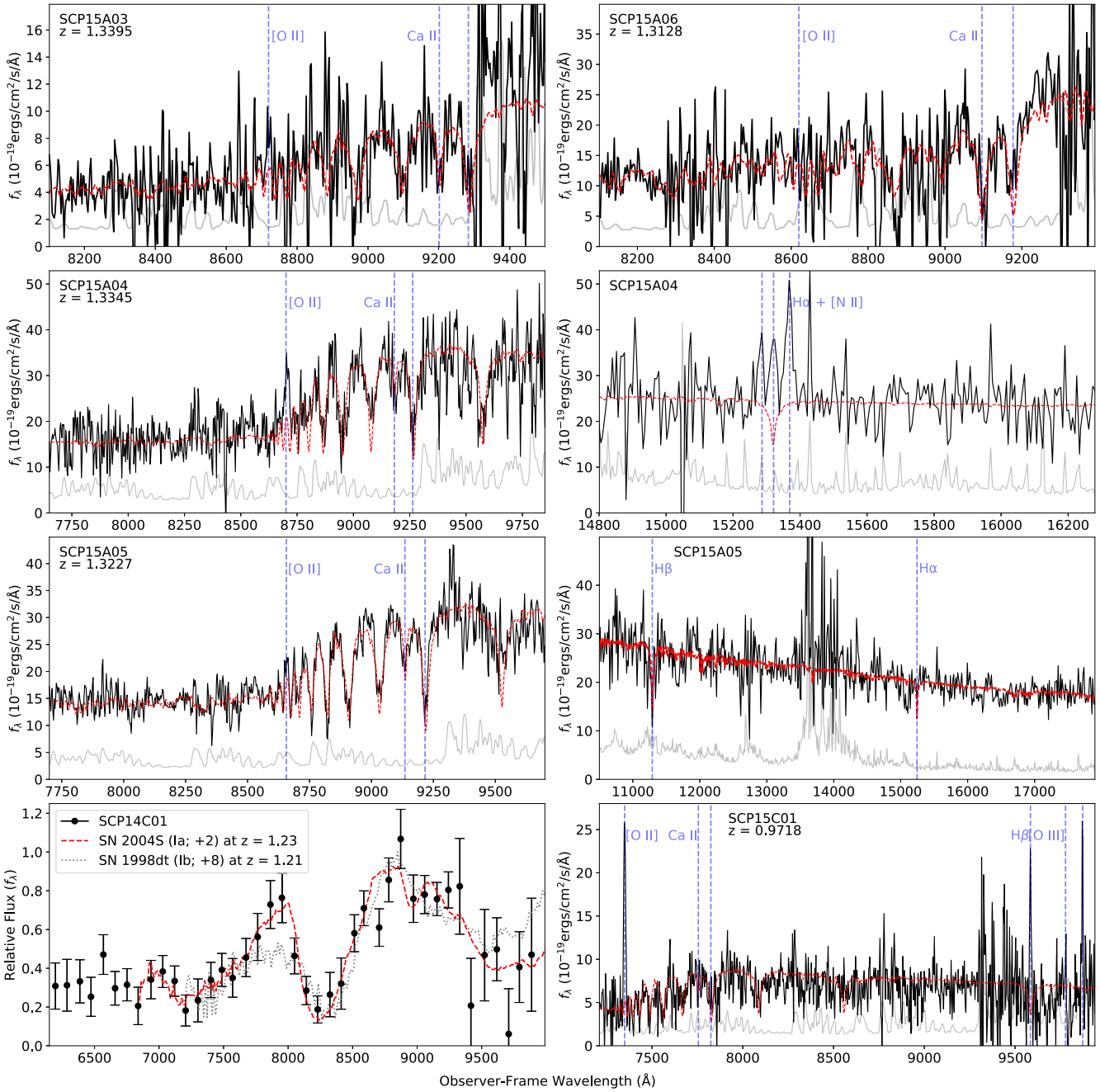

Figure 8. The VLT spectra (FORS2 and/or X-Shooter) of the host galaxies of SN Ia discovered during the See Change survey. The (solid) black line shows the data, with the errors on the spectrum shown as the (solid) grey line. The best-fitting FAST SED is shown as a (dashed) red line. The positions of selected lines are also indicated. SCP14C01 had no detected host galaxy, this spectrum being a live spectrum of the transient itself. This is compared to spectra of SN Ib 1998dt (Matheson et al. 2001; Silverman et al. 2012) and SN Ia 2004S (Krisciunas et al. 2007), with the days after peak and redshift of the comparison spectra indicated in the parentheses. The comparison spectra are simply shifted in redshift, and are not warped/adjusted in shape to match SCP14C01. For the case of SCP15D02, the red-dashed line shows the combined stellar + AGN best fit, with the stellar component of this fit shown by the red-dotted line. The spectrum of the host galaxy of possible SN Ia SCP15I02 shows tentative evidence of Na I D and Hα absorption at $z = 1.62$, near the cluster redshift of $z = 1.63$, but this is not a secure redshift.

from our X-Shooter data, and makes SCP16C03 the highest redshift SN Ia with a spectroscopic host-galaxy redshift. The photometric and spectroscopic follow-up, and a detailed analysis of SCP16C03 and its host galaxy is presented in Rubin et al. (2018).

8.3.9 SCP15D01

SCP15D01 was an SN Ia in the foreground of SPT2106. Multiple emission and absorption lines are visible in the FORS2 spectrum, from which we derive a redshift of $z = 0.5682$ for the host galaxy. Both the SED fitting and the emission lines indicate some ongoing

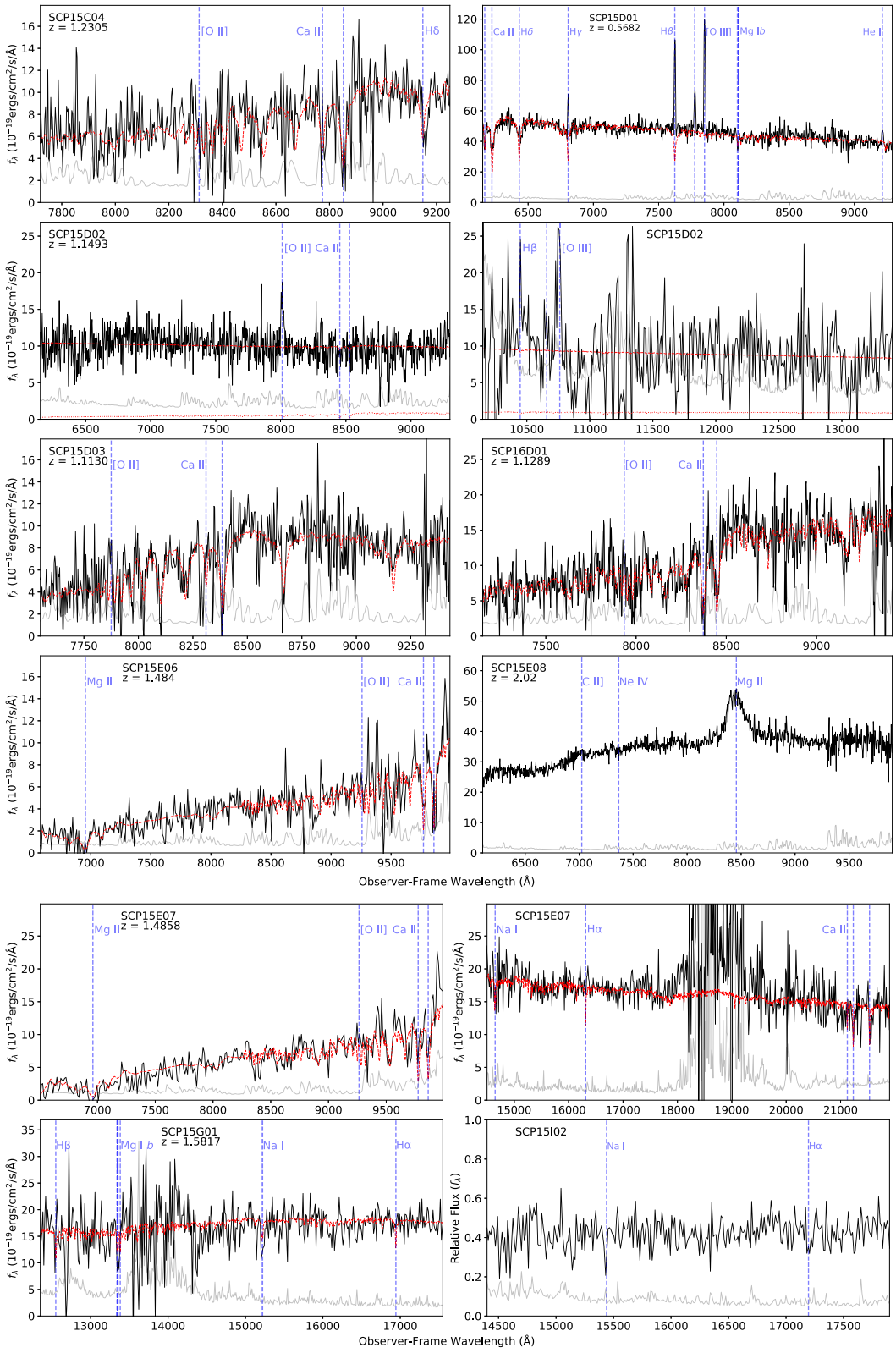

Figure 8 – *continued*

Table 5. The FAST best-fitting stellar parameters for the SCP15A04/SCP16A04 host galaxy, with and without including an AGN component in the fit.

Parameter	Without AGN	With AGN
log ($M/M_\odot$)	$10.67^{+0.14}_{-0.03}$	$10.67^{+0.22}_{-0.10}$
A_V	$1.2^{+0.2}_{-0.6}$	$0.7^{+0.5}_{-0.1}$
SFR ($M_\odot$ yr^{-1})	$0.0^{+12.3}_{-0.0}$	$0.0^{+21.4}_{-0.0}$
Stellar age (Gyr)	$0.2^{+0.5}_{-0.1}$	$0.3^{+0.1}_{-0.2}$

star formation. An SFR of $3.5^{+1.6}_{-1.3}$ $M_\odot$ yr^{-1} was derived from the SED fitting, with an SFR of 6^{+4}_{-3} $M_\odot$ yr^{-1} calculated from the strength of the Hβ emission line. While SCP15D01 is an SN Ia, it has a substantially lower redshift than our target SN Ia sample of $z \gtrsim 1$.

8.3.10 SCP15D02

SCP15D02 was a possible SN Ia in the SPT2106 cluster. The host galaxy shows significant [O II] emission at $z = 1.1493$. Furthermore, the X-Shooter NIR spectrum shows an emission-line consistent with [O III] 5007 Å at $z = 1.1493$. At this redshift, Hα is in a region of very high atmospheric absorption, so a measurement of that line is not possible. The FORS2 and X-Shooter spectra of the object can be seen in Fig. 8. The [O II] and [O III] 5007 Å emission lines are both broad for a galaxy spectrum, with FWHM ~ 700 km s^{-1}. We measure $\log([\mathrm{O\,III}]\ \lambda5007/\mathrm{H}\beta) = 0.3^{+0.2}_{-0.6}$, which does not tell us a great deal about potential AGN contribution (e.g. see Fig. 1 of Kauffmann et al. 2003). Due to this, we use the version of the FAST code that includes an AGN component in the fitting. This indicates that potentially the majority of the continuum flux in our spectra could be from an AGN, which makes the derived stellar parameters very uncertain, with a stellar age of $2.5^{+2.4}_{-2.4}$ Gyr, $\log(\mathrm{M/M}_\odot)$ of $9.29^{+2.17}_{-0.60}$ and SFR of 0^{+513}_{-0} $M_\odot$ yr^{-1}. Due the likelihood of heavy AGN contamination of the emission lines, we do not calculate SFRs from the measured emission-line fluxes.

8.3.11 SCP15D03

The host galaxy of SN Ia SCP15D03 shows several absorption lines at $z = 1.1130$, including strong Balmer absorption. The spectrum has strong Hδ absorption and is consistent with a relatively strong Balmer break. From visual inspection of Fig. 8, it appears that Ca II K does not align with the redshift. However, the redshift does agree with the other Balmer lines and potential [O II] emission. In galaxies with strong Balmer lines, Ca II K can be relatively weak (with Ca II H blended with Hϵ), due to the domination of A stars over later type stars. The SED of the SCP15D03 host is consistent with no ongoing star formation ($0.0^{+0.1}_{-0.0}$ $M_\odot$ yr^{-1}). However, there is a weak detection of [O II] emission from the spectrum, which if all associated with star formation would imply an SFR of 4^{+4}_{-2} $M_\odot$ yr^{-1}. This is higher than the SED SFR, but still consistent within 2σ. The FAST analysis indicates a stellar age of $0.8^{+0.2}_{-0.1}$ Gyr.

8.3.12 SCP15D04

It is not immediately obvious which galaxy, if any, the transient SCP15D04 is associated with. Fig. 9 shows the position of the transient, with a faint extended source within ∼1 arcsec and a much brighter source to the north. We obtained FORS2 spectroscopy of the very faint extended source slightly to the west of SCP15D04 to search for possible emission lines. However, none were found, so the redshift could not be determined. In some exposures, the slitlet went through the galaxy to the north of this faint source, with an exposure time of 3.33 h. The spectrum shows that this galaxy, labelled here SPT2106 210600.34–584545.9, is in the SPT2106 cluster, displaying strong Ca II H & K absorption at $z = 1.135$. Taking a redshift of $z = 1.135$ would imply an apparent offset of 22 kpc from SPT2106 210600.34–584545.9. SCP15D04 could therefore potentially be associated with that galaxy, even if the (apparently closer) faint extended source is not.

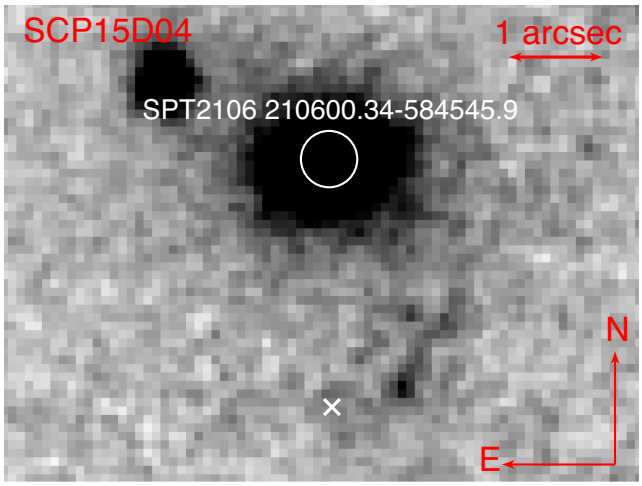

Figure 9. Stacked *HST* WFC3/IR F105W image of the region around SCP15D04. The position of the SN is indicated by a white '×'. The centre of the nearby galaxy SPT2106 210600.34–584545.9 at $z = 1.135$ is indicated by the white circle.

8.3.13 SCP16D01

The host galaxy of SCP16D01 shows the strong Ca II H & K and *G*-band absorption, along with other absorption features. We find a redshift of $z = 1.1289$ and it has a very strong cross-correlation peak, as would be expected given the strength and number of features. The spectrum of the host galaxy is shown in Fig. 8, which shows a clear 4000 Å break. The stellar age of this galaxy derived from the SED fitting is $2.5^{+0.8}_{-0.3}$ Gyr. This is significantly older than the stellar age of the SCP15D03 host in the same cluster. This can be seen in the spectra, where the SCP15D03 host shows strong Balmer absorption, rather than the strong 4000 Å break seen in the SCP16D01 host, due to the light of the former having a much stronger contribution from A stars. The SED fitting of the SCP16D01 host galaxy indicates an SFR of $0.0^{+0.3}_{-0.0}$ $M_\odot$ yr^{-1}, with an SFR of 4^{+4}_{-3} $M_\odot$ yr^{-1} derived from the weak [O II] detection.

8.3.14 SCP15E06

The FORS2 data of the SCP15E06 host galaxy shows a red continuum with Ca II H & K absorption lines, along with possible absorption from Mg II 2800 Å also seen in the spectrum, which is shown in Fig. 8. We adopt a redshift of 1.484 from the Ca II H & K lines. The cross-correlation prefers a slightly lower redshift of 1.481, however, as this conflicts with Ca II H & K (the main features that can be seen by visual inspection), we use the redshift derived from Ca II H & K alone. Compared to most of the other

objects, this has significant uncertainty in the host mass, with $\log_{10}(M/\mathrm{M}_\odot) = 10.94^{+0.29}_{-0.14}$, which in part is due to the uncertainty in the F814W *HST* photometry. The stellar age of this host is also relatively uncertain at $1.6^{+2.4}_{-0.5}$ Gyr, noting the age of the Universe at $z = 1.48$ is only 4.3 Gyr.

8.3.15 SCP15E07

We obtained both FORS2 and X-Shooter observations for the SCP15E07 host galaxy. A redshift is not immediately obvious by visual inspection. However, the cross-correlation yields a peak at $z = 1.4858$. The Ca II NIR triplet appears to be detected in the NIR data, as well as some optical features such as Ca II H & K. The combined spectrum of the SCP15E07 host are shown in Fig. 3, with zoomed-in sections of the spectrum shown in Fig. 8. We used FAST to derive a stellar age of $1.6^{+0.5}_{-0.7}$ Gyr. Both the Hα emission measurement and the FAST SED fitting indicate a low SFR for the SCP15E07 host galaxy, deriving $0.0^{+0.1}_{-0.0}$ and $0.6^{+0.4}_{-0.4}$ $\mathrm{M}_\odot\ \mathrm{yr}^{-1}$, respectively, for the two methods.

8.3.16 SCP15E08

The source near SCP15E08 has a bright continuum and a single emission line at ∼8460 Å. The emission line is very broad, with FWHM ∼6500 km s^{-1}. The source was detected as an X-ray source by XMM in 2013 (Rosen et al. 2016). Taken together, this implies that this galaxy is an AGN. As only one line is identified, the redshift is not completely secure, but the line is most likely to be Mg II 2800 Å at $z = 2.02$, which is consistent with some weaker features expected in a quasar spectrum. The continuum appears red and is likely subject to significant internal reddening. The spectrum, which is shown in Fig. 8, shows the possible presence of C II] 2326 Å, and the position of [Ne IV] is added for reference. Note that the 2175 Å extinction bump would be blueward of C II] 2326 Å. This is often not seen in quasar spectra (Pitman, Clayton & Gordon 2000), but has been detected in some case (e.g. Jiang et al. 2011), so caution should be excersized in interpreting broad changes in the continuum here. The photometry of SCP15E08 is consistent with an SN Ia, likely at a higher redshift than the cluster ($z > 1.6$), and is indeed consistent with an SN Ia at $z = 2.02$. The transient is not coincident with the centre of the AGN, so the new object is not due to variability in the central source itself.

8.3.17 SCP15G01

A redshift of $z = 1.5817$ was obtained for the SCP15G01 host galaxy, mainly from Keck data (Hayden et al., in preparation). Using this redshift, we can put limits on the Hα emission with our VLT data. At this redshift, the region of the Ca II H & K lines has very poor sensitivity in X-Shooter. However, using this redshift, there does appear to be possible absorption from Na I D and Mg *b*. The FAST SED analysis indicates that this is a massive galaxy, with $\log_{10}(M/\mathrm{M}_\odot) = 11.44^{+0.03}_{-0.15}$. The spectrum shows no obvious evidence of Hα emission. A forced measurement of the excess Hα flux over the fitted continuum yields $5.5 \pm 3.8 \times 10^{-18}$ erg s^{-1}, implying SFR of $1.6^{+2.7}_{-1.3}$ $\mathrm{M}_\odot\ \mathrm{yr}^{-1}$, consistent with the FAST rate of $0.0^{+17.4}_{-0.0}$ $\mathrm{M}_\odot\ \mathrm{yr}^{-1}$. The VLT spectrum is shown in Fig. 8. The SED indicates a stellar age of $4.0^{+0.0}_{-2.0}$ Gyr, where the age of the Universe at $z = 1.5817$ sets the upper limit on the stellar age.

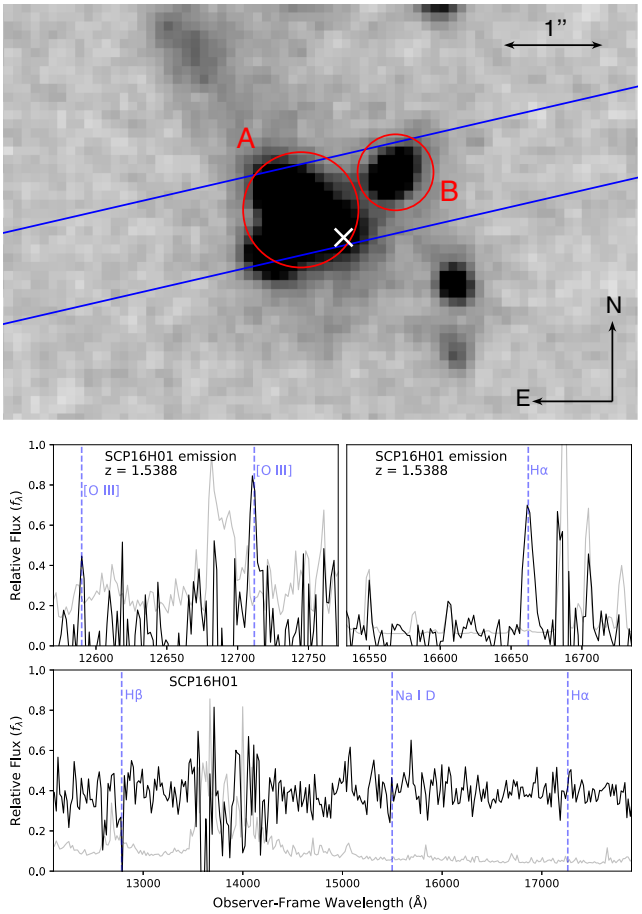

Figure 10. Upper panel: stacked *HST* WFC3/IR F105W image showing the host structure of SCP16H01. The two components with spectra are indicated in red (see the text), the position of the X-Shooter slit is in blue and the position of SN Ia SCP16H01 is indicated by a white '×'. Middle panel: X-Shooter spectrum of Component B of the SCP16H01 host structure, showing Hα and [O III] 5007 Å emission at $z = 1.5388$. Lower panel: X-Shooter spectrum of Component A of the SCP16H01 host structure, showing no secure redshift, with the expected positions of lines placed at the cluster redshift ($z = 1.63$) indicated for reference. This spectrum is corrected for contamination by Component B. Key as given in Fig. 6.

8.3.18 SCP16H01

The X-Shooter spectrum of the SCP16H01 host galaxy shows two components; the main continuum and emission lines slightly offset (in the spatial direction) from the continuum. The structure can be seen in Fig. 10, with the position of the SN also indicated. The continuum is from component 'A' and the Hα and [O III] 5007 Å emission lines are from component 'B'. The accompanying [O III] 4959 Å line is possibly present as well, but the larger errors and weakness of the line make this only tentative. This gives a redshift for component B of $z = 1.5388$, which places the galaxy in the foreground of the cluster. These emission lines from component B are very narrow, with the strongest line, Hα, measured at FWHM ∼100 km s^{-1} after correcting for spectral resolution. This spectrum can be seen in Fig. 10. Any possible contamination from the emission-line object was subtracted from the main trace using the half of the emission-line trace furthest spatially from the main trace. This may also subtract a small percentage of the main trace flux ($\lesssim$5 per cent). The errors are fully propagated through this subtraction, but do not increase significantly due to the optimal

extractions employed; i.e. where the flux from the emission-line object is strongest spatially has a reasonable offset from the centre of the main trace and thus the flux/error at this pixel has a low weighting in the optimal combining. The spectrum of component A, after removal of the contamination, shows no evidence of features at the same redshift as component B. In conclusion, from the imaging we can see the SN is likely associated with component A, but the spectroscopic redshift of that component remains inconclusive.

8.3.19 SCP15I02

The host galaxy of possible SN Ia SCP15I02 has a detected continuum. However, we have not been able to obtain a secure redshift from the data. The spectrum is shown in Fig. 8 and shows possible evidence of Na I D absorption near the cluster redshift of 1.63. At this redshift, X-Shooter has low sensitivity in the region of Ca II H & K.

9 DISCUSSION

Our observing strategy for obtaining spectroscopic redshifts was partially focused on emission-line fluxes; Hα with X-Shooter and [O II] with FORS2. The lack of strong emission lines found in these $z > 1$ galaxies meant that obtaining the redshifts was more challenging, as we had to rely on absorption lines and therefore required higher S/N on the galaxy continuum. In the cases of the lowest luminosity hosts, obtaining a spectroscopic redshift was not possible. We have, however, been been able to obtain redshifts for 15 SNe Ia and one possible SN Ia at $z \gtrsim 1$. In total, 13 of these 16 transients were in the target clusters, in addition to one in the foreground and two in the background. Looking towards future surveys, this shows that it is possible to obtain spectroscopic redshifts for the majority of SNe Ia in cluster environments through host spectroscopy in the $1 < z < 1.5$ range. This often requires several hours of exposure, even on 8−10- m class telescopes.

As well as their use in the cosmological analysis, these redshifts were often needed to classify the transients. At these high redshifts, a live transient spectrum was typically not feasible, due to a combination of the heavy telescope time investment that would have been required, the difficulty scheduling such long observations when the SN was at peak and coinciding with optimal observing conditions. The full transient classifications will be presented in Hayden et al. (in preparation). We also obtained redshifts for most of the other transients discovered through See Change. Indeed the redshifts for these objects were sometimes needed to rule them out as cluster SNe Ia, for example, to break a degeneracy from a light curve that could be consistent with a cluster SN Ia or a foreground CC SN (e.g. SCP15C02; Hayden et al. in preparation).

9.1 Cluster environments of the SNe Ia

A clear result of our $z \gtrsim 1$ cluster SN Ia host spectroscopy is the apparent lack of star formation from the FAST SED fitting. There are only two cluster SN Ia host galaxies with emission lines detected with $>3\sigma$ significance, the hosts of SCP15A04/16A04 and SCP15D02, both of which show evidence of AGN activity in the spectrum. The foreground $z = 0.9718$ SCP15C01 host galaxy also shows significant [O II] and Hβ emission.

Another interesting result of the See Change programme is that some clusters show higher rates of detected SNe Ia than others. The three SPT clusters have produced more than half of the cluster SNe Ia, likely SNe Ia or possible SNe Ia found by See Change. The number of SNe Ia in each See Change cluster that was also a potential VLT target are summarized in Table 6. Of the 39 See Change transients that we attempted to obtain a VLT spectroscopic redshift, we were successful for 26 of those. For each cluster, we summarize the galaxy parameters that we derive for the cluster SN Ia host galaxies below, and how they compare to other cluster members. The majority of the spectroscopic follow-up of the objects not feasible to target with the VLT (i.e. Dec. $\gg 0^\circ$) was done at the Keck observatory. The redshifts and stellar masses of these objects will be presented in a future publication.

Table 6. Summary of the number of SNe Ia, likely SN Ia or possible SNe Ia in each cluster (not including those in the foreground or background), and the number of those for which we were able to derive a spectroscopic redshift.

Cluster (designation)	Redshift	SNe Ia	SNe Ia with spec-z
SPT2106 (D)	1.13	4	3
MOO1014 (C)	1.23	2	2
SPT0205 (A)	1.32	6	5
SpARCS0035 (F)	1.34	0	0
SPT2040 (E)	1.48	4	2
XDCP0044 (G)	1.58	1	1
SpARCS0224 (I)	1.63	2	1
SpARCS0330 (H)	1.63	1	0
Total		20	14

Notes. The numbers for the cluster SNe Ia without a spectroscopic redshift are from the number of SNe Ia that have a photometric redshift consistent with the SN Ia residing in the observed galaxy cluster. We note that the one host galaxy with a spectroscopic redshift in cluster SpARCS0224 was not observed with VLT.

SPT0205 had six SNe Ia detected. None of the SN Ia host galaxies in SPT0205 show strong emission lines. The strongest lines are those seen in the host of SCP15A04/SCP16A04. The high [N II] λ6583/Hα ratio in this galaxy indicates they are likely influenced by AGN activity. In the four cluster SN Ia host galaxies analysed in this work, we find stellar ages of $0.2^{+0.5}_{-0.1}$, $1.0^{+1.0}_{-0.3}$, $1.0^{+0.3}_{-0.8}$, and $1.3^{+1.9}_{-0.3}$ Gyr. In their analysis of this cluster, Stalder et al. (2013) concluded that the majority of the star formation took place at $z > 2.5$. At the redshift of SPT0205, $z = 2.5$ corresponds to an age of ∼2.1 Gyr. Our results therefore imply that there has been more recent star formation in at least some members of this cluster. The hosts of SCP15A03, SCP15A04 (+ SCP16A04), and SCP15A05 all show strong high-order Balmer absorption. The SCP15A04 host is the only galaxy where [O II] is detected at $>3\sigma$ significance, but we know from the [N II]/Hα ratio that at least some of this will likely come from AGN activity. The spectra of these three host galaxies are consistent with post-starburst spectra. The only spectrum where the Ca II H & K/4000-Å break is more prominent in the spectra than the Balmer absorption lines is the host of SCP15A06. This is different to the spectra published by Stalder et al. (2013, see their fig. 3), where, in general, the Ca II H & K/4000-Å break were the strongest features seen in the galaxies they observed. This could be a selection effect, given that the nine galaxy spectra published by Stalder et al. (2013) were the only ones confirmed from 47 slits of their spectroscopic observations and thus likely to be brighter/more massive. In contrast, our target was to observe the specific galaxies that happened to host an SN Ia during the See Change survey. Another possible contributing factor is the delay-time distribution of SNe Ia, where the SN Ia rate is dependent on the time since the hosting stellar population was formed (see e.g. Totani et al. 2008).

This, in turn, would cause a correlation between the global stellar age of a galaxy and the relative SN Ia rate.

SPT2106 produced two SNe Ia, plus a possible SN Ia. As with SPT0205, the majority of confirmed cluster members in SPT2106 appear to be passive, with no obvious [O II] detection (Foley et al. 2011). Of our three SN host galaxies, only SCP15D02 shows strong [O II] and [O III] emission, with the emission lines being relatively broad and likely affected by AGN activity. The hosts of SCP15D03 and SCP16D01 show significantly different stellar populations. The spectrum of the SCP15D03 host galaxy shows a much younger population ($0.8^{+0.2}_{-0.1}$ Gyr) than that of SCP16D01 ($2.5^{+0.8}_{-0.3}$ Gyr), with the latter being $\sim$ eight times more massive than the former.

SPT2040 had two cluster SNe Ia and one background SN Ia that we were able to obtain redshifts for. In addition, there was a likely SN Ia and possible SN Ia for which we were not able to obtain a redshift. The FORS2 follow-up of galaxies in this cluster was challenging, as with the cluster redshift at $z = 1.478$, the positions of Ca II H & K are red enough for the efficiency of the detector to be significantly reduced. However, we have been able to obtain redshifts for cluster SNe Ia SCP15E06 and SCP15E07, the latter with the aid of X-Shooter data. The hosts of both SCP15E06 and SCP15E07 appear passive from the SED fitting, and have no detected [O II] emission. A weak Hα detection indicates a low SFR of $0.6 \pm 0.4\,\mathrm{M_\odot\,yr^{-1}}$ for the host galaxy of SCP15E07. This is in contrast to the other confirmed cluster members, with Bayliss et al. (2014) finding significant ongoing star formation in SPT2040. They identified 15 cluster members, all of which showed [O II] emission. This is from observations from 59 slits, implying a successful detection rate of [O II] of 25 ± 7 per cent, significantly higher than that found in SPT0205 and SPT2106, which both had [O II] detection rates of 2 ± 2 per cent (Bayliss et al. 2014). However, the authors note that their SPT2040 spectra were not sufficiently sensitive to pick up Ca II H & K, implying a large bias towards finding emission-line galaxies – i.e. the 15 galaxies confirmed are not necessarily a representative sample of the average cluster galaxy. Note that this caveat does not affect the above [O II] detection rate comparison made by Bayliss et al. (2014). However, it does show that no conclusion can be drawn from the fact that, unlike the previously confirmed members, our two SN Ia hosts in SPT2040 appear relatively passive, and indeed a meaningful comparison to our spectra is not possible. The implied stellar ages of the two galaxies are $1.6^{+0.5}_{-0.7}$ and $1.6^{+2.4}_{-0.5}$ Gyr. In addition to the cluster SNe Ia, we have also identified a background SN Ia in the field of SPT2040, occurring in a broad-lined AGN host galaxy at $z = 2.02$, SCP15E08.

MOO1014 only has one cluster SN for which we have been able obtain a host spectrum. The spectrum shows Ca II H & K with evidence of a 4000-Å break. The SED fitting indicates an old stellar population, with the best-fitting stellar age of $4.0^{+0.0}_{-1.6}$ Gyr. The spectra of the two additional cluster galaxies that we confirm (but did not host an SN Ia; shown if Fig. 6) also show strong Ca II H & K absorption and evidence of a 4000-Å break.

The host galaxy of SCP15G01 does not show strong emission lines and the SED is consistent with an old stellar population, with a stellar age of $4.0^{+0.0}_{-2.0}$ Gyr. Of the three spectra of cluster XDCP0044 presented by Santos et al. (2011), two show [O II] emission.

9.2 Stellar mass and SFR measurements

We used FAST SED fitting on a combination of the *HST* photometry and VLT spectroscopy for each of the SN Ia host galaxies for which a secure spectroscopic redshift has been obtained. The derived stellar mass, internal extinction (A_V), SFR, sSFR, and stellar age for each host is listed in Table 7, along with SFR parameters as derived from the emission-line constraints on each host galaxy. We do not analyse the host of SCP15E08, as much of the light detected in the spectrum will originate from the central source, rather than the stellar population. The upper panel of Fig. 11 shows a histogram of the masses derived from FAST for the $z \gtrsim 1$ SNe Ia. If we take the cut-off in the 'mass step' to be $\log[M/\mathrm{M_\odot}] = 10$ from Sullivan et al. (2010) we find 10.5 ± 0.5 (SCP5D03 could be in either bin) of the 12 SNe Ia with a host spectroscopic redshift are in the upper mass bin. If we take the cut-off as 10.5 from Roman et al. (2018), we find 9 ± 1 of the 12 are in the upper mass bin. We exclude the possible SN Ia SCP15D02 from these numbers, due to its highly uncertain stellar mass. If we include the apparently hostless SCP14C01 in here, this of course adds one to the low stellar mass bin. The uncertainties in the derived stellar masses are generally around 0.1–0.2 dex, sufficiently accurate to unambiguously determine which side of the mass-step an object lies in most cases.

In the lower panel of Fig. 11, we show a comparison of the sSFRs derived via the emission lines and those derived via FAST SED fitting. In four cases the emission-line sSFRs are higher (by $>1\sigma$) than those derived from the SED fitting. In each of these cases (SCP15A03, SCP15D03, SCP16D01, and SCP15E07), the emission-line measurements themselves represent a $<3\sigma$ detection, however, when taken together, they could indicate emission-line contamination from sources unrelated to recent star formation. If one is adding a step-type function into SN Ia standardization, it only matters which side of this step they lie on. For example, significant differences in the sSFR derived from the SED and emission lines would not matter if both indicated $\log[\mathrm{sSFR}] < -9.7$. The sSFRs are generally more poorly constrained than the stellar masses, particularly the sSFR measurements derived from the emission lines.

We have shown that the combination of *HST* photometry and VLT spectroscopy gives sufficiently good constraints on the stellar mass of each host galaxy to reveal which 'mass bin' the host lies in, and thus allowing a correction for the Hubble residuals to be made in the cosmological analysis. This could be particularly important for the See Change survey due the passive environments of the majority of galaxies, meaning the distribution of host galaxy environments will likely differ significantly to that explored in many other surveys.

We find the sSFRs to generally be well constrained by the SED fitting of the VLT spectra and *HST* photometry, and which side of the sSFR step they reside can usually be determined. The SFRs derived from the emission-line measurements are generally more poorly constrained than from the SED fitting. This is in part due to the fact that we often had to rely on an [O II] measurement for the SFR estimate. At 3727 Å, [O II] is more sensitive to extinction, and in many galaxies the extinction itself is not tightly constrained, making the uncertainty on the SFR much higher than the direct measurement on the observed emission-line strength. There is evidence that emission lines in some of the host galaxies may be contaminated by sources not associated with star formation, although for individual galaxies the evidence is not significant. For these reasons, we conclude that the SFRs derived from the SED fitting are likely to be generally more accurate and precise.

The average uncertainty in the distance modulus for the See Change SNe Ia is $\sim$0.2 mag (Hayden et al., in preparation). The mass step was measured as 0.07 mag by Roman et al. (2018). With a sample of 27 cosmologically-useful SNe Ia or likely SNe Ia, and with the host environments being different to many other SN Ia

Table 7. Summary of the properties of the galaxies that hosted SNe Ia (note SCP15D02 is only classified as a possible SN Ia), where a redshift could be determined, excluding the host of SCP15E08.

Host	Redshift	$\log_{10}(M/M_\odot)$	A_V	SED SFR ($M_\odot\,yr^{-1}$)	Emission SFR ($M_\odot\,yr^{-1}$)	$\log_{10}(sSFR_{SED})$	$\log_{10}(sSFR_{EL})$	Stellar age (Gyr)
SCP15A03	1.3395 ± 0.0003	$10.56^{+0.05}_{-0.11}$	$0.8^{+0.1}_{-0.4}$	$0.0^{+0.3}_{-0.0}$	12^{+7}_{-10} ([O II])	<-10.8	$-9.5^{+0.2}_{-0.7}$	$1.0^{+1.0}_{-0.3}$
SCP15A04	1.3345 ± 0.0001	$10.67^{+0.14}_{-0.03}$	$1.2^{+0.2}_{-0.6}$	$0.0^{+12.3}_{-0.0}$	23^{+11}_{-16} (Hα)	<-9.3	$-9.3^{+0.2}_{-0.7}$	$0.2^{+0.5}_{-0.1}$
SCP15A05	1.3227 ± 0.0002	$10.63^{+0.04}_{-0.12}$	$0.5^{+0.4}_{-0.2}$	$5.1^{+0.0}_{-5.1}$	$0.7^{+0.9}_{-0.6}$ (Hα)	$-9.9^{+0.0}_{-2.6}$	$-10.8^{+0.4}_{-0.7}$	$1.0^{+0.3}_{-0.8}$
SCP15A06	1.3128 ± 0.0005	$11.07^{+0.30}_{-0.01}$	$0.3^{+0.6}_{-0.1}$	$0.0^{+0.1}_{-0.0}$	<8.4 ([O II])	$-13.3^{+1.3}_{-\text{unc.}}$	<-10.1	$1.3^{+1.9}_{-0.3}$
SCP15C01	0.9718 ± 0.0002	$9.56^{+0.07}_{-0.19}$	$0.8^{+0.4}_{-0.8}$	$0.2^{+2.4}_{-0.2}$	12^{+17}_{-10} (Hβ)	$-9.4^{+0.3}_{-\text{unc.}}$	$-8.5^{+0.4}_{-0.9}$	$0.6^{+0.7}_{-0.4}$
SCP15C04	1.2305 ± 0.0003	$10.45^{+0.09}_{-0.16}$	$0.2^{+0.1}_{-0.2}$	$2.2^{+0.9}_{-1.4}$	<0.9 ([O II])	$-10.1^{+0.1}_{-0.3}$	<-10.4	$4.0^{+0.0}_{-1.6}$
SCP15D01	0.5682 ± 0.0001	$9.87^{+0.08}_{-0.06}$	$0.5^{+0.2}_{-0.2}$	$3.5^{+1.6}_{-1.3}$	6^{+4}_{-3} (Hβ)	$-9.3^{+0.2}_{-0.2}$	$-9.1^{+0.2}_{-0.3}$	$4.0^{+3.9}_{-2.3}$
SCP15D02	1.1493 ± 0.0002	$9.29^{+2.17}_{-0.60}$	$1.6^{+0.3}_{-0.3}$	0^{+513}_{-0}	–	<-7.1	–	$2.5^{+2.4}_{-2.4}$
SCP15D03	1.1130 ± 0.0003	$9.98^{+0.06}_{-0.03}$	$0.5^{+0.2}_{-0.1}$	$0.0^{+0.1}_{-0.0}$	4^{+4}_{-2} ([O II])	<-10.8	$-9.4^{+0.3}_{-0.4}$	$0.8^{+0.2}_{-0.1}$
SCP16D01	1.1289 ± 0.0002	$10.89^{+0.04}_{-0.05}$	$0.5^{+0.2}_{-0.1}$	$0.0^{+0.3}_{-0.0}$	4^{+4}_{-3} ([O II])	<-12.1	$-10.3^{+0.3}_{-0.4}$	$2.5^{+0.8}_{-0.3}$
SCP15E06	1.484 ± 0.003	$10.94^{+0.29}_{-0.14}$	$0.5^{+0.7}_{-0.3}$	$0.0^{+0.4}_{-0.0}$	<21 ([O II])	<-11.1	<-9.6	$1.6^{+2.4}_{-0.5}$
SCP15E07	1.4858 ± 0.0003	$11.03^{+0.02}_{-0.10}$	$0.2^{+0.1}_{-0.1}$	$0.0^{+0.1}_{-0.0}$	$0.6^{+0.4}_{-0.4}$ (Hα)	$-13.5^{+1.4}_{-\text{unc.}}$	$-11.2^{+0.2}_{-0.4}$	$1.6^{+0.5}_{-0.7}$
SCP15G01	1.5817 ± 0.0004	$11.44^{+0.03}_{-0.15}$	$0.7^{+0.5}_{-0.3}$	$0.0^{+17.4}_{-0.0}$	$1.6^{+2.7}_{-1.3}$ (Hα)	<-9.8	$-11.2^{+0.4}_{-0.7}$	$4.0^{+0.0}_{-2.0}$

Notes. The uncertainties on the redshifts are derived from the cross-correlation, with the exception of SCP15E06 (difference between visual inspection redshift and that from cross-correlation). We take the minimum uncertainty to be $\Delta z = \pm 0.0001$, even though the cross-correlation gives a more precise result in a few cases. The parameters are derived from emission-line measurements from the VLT spectra and the SED fitting performed by FAST. $sSFR_{SED}$ is derived from the SFR determined by the FAST SED fitting of the stellar spectra and photometry, whereas $sSFR_{EL}$ is derived from the emission-line SFR measurement. Both measurements use the stellar mass from FAST. Upper limits indicate 95% confidence and 'unc.' = unconstrained. All SFR measurements are corrected for extinction, but do not consider contamination by AGN activity or post-AGB stars.

surveys, it will therefore be important to consider the host masses when conducting the final cosmological analysis.

As an example, we take the uncertainty on each SN to be ∼0.2 mag, plus an intrinsic uncertainty on the distance modulus (i.e. that which arises from SNe Ia not being perfectly standardizable) to be ∼0.1 mag. If we combine 27 such SNe Ia (at the same redshift), we would get an combined uncertainty on the distance modulus of ∼0.04 mag. Thus if all SNe were on one side of the mass step (and assuming the mass step does not evolve with redshift), the offset arising from the mass step would be of similar order to the uncertainly. This is obviously a very simplistic picture as: (a) the See Change SNe Ia range from $z = 0.86$ to 2.29 (Hayden et al., in preparation), and (b) the hosts are not all on one side of the mass step, as we have shown in this work. However, it does illustrate that such a correction needs to be considered for a sample the size of See Change.

In this work, we derived galaxy parameters from SED fitting of a combination of our spectra and the *HST* photometry. In Fig. 12, we compare these values to those derived using a combination of the *HST* photometry and the spectroscopic redshift, but not using the spectra themselves in the fitting. This shows that the uncertainty in the parameters is significantly reduced using the spectra. The stellar ages and reddening are very poorly constrained from the photometry (not included in Fig. 12), as one would expect given the degeneracy between the two parameters from photometry alone. The estimates on the sSFRs with *HST* photometry and spectroscopic redshifts are poorly constrained, with it generally not being possible to determine which side of any sSFR 'step' that an individual galaxy would lie. The *HST* photometry and spectroscopic redshifts do, however, provide reasonable estimates on the stellar masses. In terms of reducing the telescope time used, this would be useful in the case of emission-line galaxies, where one could potentially confirm the redshift without significant S/N on the continuum. However, in the case of low-SFR environments like most of our sample, reasonable S/N is needed on the continuum to detect absorption lines and confirm the redshift. Therefore, in such cases, no extra telescope time is actually required to significantly improve the stellar mass estimates and other parameters.

10 SUMMARY AND CONCLUSIONS

In this paper, we have presented VLT spectra of the host galaxies of transients discovered in the See Change survey, including the hosts of 15 SNe Ia and one possible SN Ia at redshifts $z > 0.97$. We now summarize our main findings:

(i) The See Change survey targeted massive galaxy clusters at $1.13 \leq z \leq 1.75$ to observe SNe Ia.

(ii) The primary aim of the work presented here was to obtain secure redshifts of the host galaxies of the $z \gtrsim 1$ SNe Ia found in the survey for use in a cosmological analysis and SN typing of the objects themselves.

(iii) We targeted 39 transients with the VLT and successfully obtained redshifts for 26 of those. Of these, 15 are classified as $z \gtrsim 1$ SNe Ia, plus one possible SN Ia, which is approximately two-thirds of the See Change SNe Ia with spectroscopic redshifts.

(iv) The majority of host galaxies did not show strong [O II] 3727 Å emission, consistent with many of the other confirmed galaxies in these massive clusters also being mainly passive.

(v) Combining these spectra with *HST* photometry, we have used FAST to derive parameters for each SN Ia host galaxy, including stellar mass, SFR, and stellar age.

(vi) The uncertainties in the FAST stellar masses are generally relatively small, allowing us to determine which side of the mass step each object lies. This will allow a correction to be made when performing a cosmological analysis.

(vii) In the case of SNe Ia (plus the possible SN Ia SCP15D02) at $0.97 \leq z \leq 1.5$ (i.e. where [O II] and Ca II H & K are still at

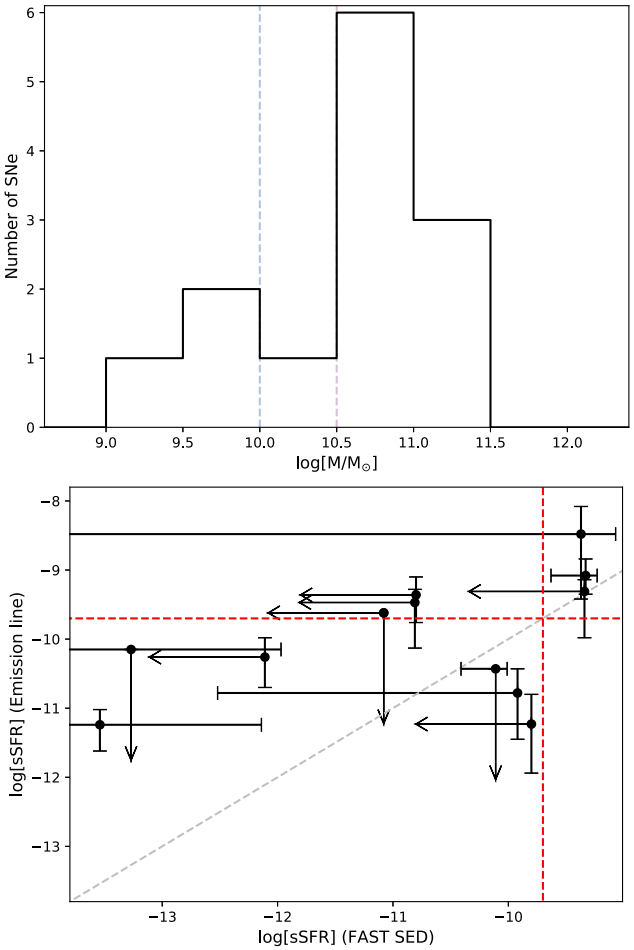

Figure 11. Top panel: histogram (solid black line) of the masses derived by FAST, with the cut-offs in the 'mass step' of log[M/M$_\odot$] of 10 (light blue Sullivan et al. 2010) and 10.5 (light purple Roman et al. 2018) also indicated. As it hosted two SNe Ia, SCP15A04 is counted twice here. Bottom panel: comparison between the sSFR derived from the emission lines, and those derived from the FAST SED fitting. The grey-dashed line indicates where the two sSFR measurements are equal and the red-dashed lines indicate the cutoff between the two log[sSFR] bins of −9.7 (Sullivan et al. 2010). We include the SCP15D01 host galaxy in the sSFR comparison, but as it is at a comparatively low z, we do not include it in the stellar-mass histogram.

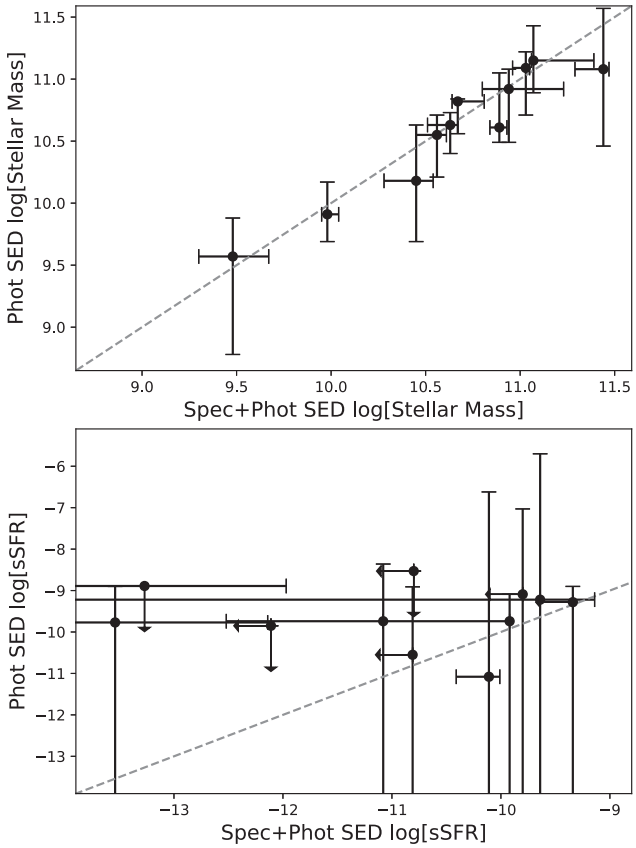

Figure 12. Comparison between galaxy parameters derived from SED fitting using our spectra and the *HST* photometry to those using just the *HST* photometry and spectroscopic redshift (but not the spectra themselves). We show comparisons for stellar mass (upper panel) and sSFR (lower panel). Due to the highly uncertain stellar parameters, the SCP15D02 host galaxy is not included in these plots. We also do not include SCP15D01 as it has a substantially lower redshift than our target range.

<1μm), we successfully obtained a redshift for 13 out of the 17 attempted with the VLT. We have therefore shown that even for passive galaxies, it is possible to obtain secure redshifts for the majority of SNe Ia found in galaxy clusters out to $z = 1.5$.

(viii) Confirming the redshifts of these cluster SN Ia host galaxies does, however, require significant time, even on 8−10-m class telescopes, with typical required total exposure times around 3−4 h.

(ix) In total, 15 objects for which we obtained a redshift are able to be classified as $z \gtrsim 1$ SNe Ia. This includes one in a broad-lined AGN host galaxy at $z = 2.02$ and a lensed SN Ia in a passive galaxy at $z = 2.22$ (reported by Rubin et al. 2018).

From the See Change survey, we have already published a paper on a $z = 2.22$ SN Ia, lensed by the MOO1014 cluster (Rubin et al. 2018). Several papers that utilize See Change data to study the clusters themselves have also been published. An overview of the See Change survey itself will be presented by Hayden et al. (in preparation). The cosmological analysis in currently ongoing and will be presented by Hayden et al. (in preparation).

ACKNOWLEDGEMENTS

SCW and IMH acknowledge support from STFC consolidated grants ST/P00038X/1 and ST/R000514/1. We acknowledge an anonymous referee for comments that improved the quality of this paper. This work is based on observations collected at the European Organisation for Astronomical Research in the Southern Hemisphere under ESO programmes 294.A-5025(A), 095.A-0830(A, B, C), 096.A-0926(B, C), 097.A-0442(A, B, C), and 0100.A-0851(A). We thank the ESO staff for assisting with observation planning. This work is also based on observations made with the NASA/ESA *HST*, obtained at the Space Telescope Science Institute, which is operated by the Association of Universities for Research in Astronomy, Inc., under NASA contract NAS 5-26555. These observations are associated with programs GO-13677 and GO-14327, along with GO-13747. This paper makes use of data obtained at the W. M. Keck Observatory, which is operated as a scientific partnership among the California Institute of Technology, the University of California, and the National Aeronautics and Space Administration. The Observatory was made possible by the generous financial support of the W. M. Keck Foundation.

REFERENCES

Abbott T. M. C. et al., 2019, ApJ, 872, L30
Adelman-McCarthy J. K. et al., 2007, ApJS, 172, 634
Aird J., Coil A. L., Georgakakis A., 2017, MNRAS, 465, 3390
Aird J., Coil A. L., Georgakakis A., 2018, MNRAS, 474, 1225
Appenzeller I. et al., 1998, The Messenger, 94, 1
Barbary K., 2016, J Open Source Softw., 1, 58
Barbary K. et al., 2012, ApJ, 745, 32
Bayliss M. B. et al., 2014, ApJ, 794, 12
Belfiore F. et al., 2016, MNRAS, 461, 3111
Bertin E., Arnouts S., 1996, A&AS, 117, 393
Bleem L. E. et al., 2015, ApJS, 216, 27
Blondin S., Tonry J. L., 2007, ApJ, 666, 1024
Brammer G. B., van Dokkum P. G., Coppi P., 2008, ApJ, 686, 1503
Brodwin M. et al., 2015, ApJ, 806, 26
Calzetti D., Armus L., Bohlin R. C., Kinney A. L., Koornneef J., Storchi-Bergmann T., 2000, ApJ, 533, 682
Calzetti D. et al., 2010, ApJ, 714, 1256
Cardelli J. A., Clayton G. C., Mathis J. S., 1989, ApJ, 345, 245
Chornock R. et al., 2013, ApJ, 767, 162
Decker B. et al., 2019, ApJ, 878, 72
Delahaye A. G. et al., 2017, ApJ, 843, 126
Fassbender R. et al., 2014, A&A, 568, A5
Foley R. J. et al., 2011, ApJ, 731, 86
Foltz R. et al., 2018, ApJ, 866, 136
Freudling W., Romaniello M., Bramich D. M., Ballester P., Forchi V., García-Dabló C. E., Moehler S., Neeser M. J., 2013, A&A, 559, A96
Ganeshalingam M., Li W., Filippenko A. V., 2013, MNRAS, 433, 2240
Gonzalez A. H. et al., 2015, ApJ, 812, L40
Gonzalez A. H. et al., 2019, ApJS, 240, 33
Guillochon J., Parrent J., Kelley L. Z., Margutti R., 2017, ApJ, 835, 64
Guy J. et al., 2007, A&A, 466, 11
Guy J. et al., 2010, A&A, 523, A7
Hamuy M., Phillips M. M., Maza J., Suntzeff N. B., Schommer R. A., Aviles R., 1995, AJ, 109, 1
Hicken M., Wood-Vasey W. M., Blondin S., Challis P., Jha S., Kelly P. L., Rest A., Kirshner R. P., 2009, ApJ, 700, 1097
Hildebrandt H. et al., 2010, A&A, 523, A31
Horne K., 1986, PASP, 98, 609
Hubble E., 1929, Proc. Natl. Acad. Sci., 15, 168
Jee M. J., Ko J., Perlmutter S., Gonzalez A., Brodwin M., Linder E., Eisenhardt P., 2017, ApJ, 847, 117
Jiang P., Ge J., Zhou H., Wang J., Wang T., 2011, ApJ, 732, 110
Jones D. O. et al., 2018, ApJ, 867, 108
Kauffmann G. et al., 2003, MNRAS, 346, 1055
Kausch W. et al., 2015, A&A, 576, A78
Kelson D. D., Martini P., Mulchaey J. S., 2003, Optimal Measurements of Redshifts Using the Weighted Cross-Correlation, available at https://code.obs.carnegiescience.edu/Algorithms/realcc
Kessler R. et al., 2009, PASP, 121, 1028
Kewley L. J., Dopita M. A., Sutherland R. S., Heisler C. A., Trevena J., 2001, ApJ, 556, 121
Kewley L. J., Geller M. J., Jansen R. A., 2004, AJ, 127, 2002
Kriek M., van Dokkum P. G., Labbé I., Franx M., Illingworth G. D., Marchesini D., Quadri R. F., 2009, ApJ, 700, 221
Krisciunas K. et al., 2007, AJ, 133, 58
Lidman C. et al., 2012, MNRAS, 427, 550
Matheson T., Filippenko A. V., Li W., Leonard D. C., Shields J. C., 2001, AJ, 121, 1648
Meyers J. et al., 2012, ApJ, 750, 1
Miknaitis G. et al., 2007, ApJ, 666, 674
Morokuma T. et al., 2010, PASJ, 62, 19
Mosher J. et al., 2014, ApJ, 793, 16
Muzzin A. et al., 2009, ApJ, 698, 1934
Muzzin A., Wilson G., Demarco R., Lidman C., Nantais J., Hoekstra H., Yee H. K. C., Rettura A., 2013, ApJ, 767, 39
Neill J. D. et al., 2009, ApJ, 707, 1449
Noble A. G. et al., 2017, ApJ, 842, L21
Perlmutter S. et al., 1999, ApJ, 517, 565
Phillips M. M., 1993, ApJ, 413, L105
Pitman K. M., Clayton G. C., Gordon K. D., 2000, PASP, 112, 537
Poznanski D., Gal-Yam A., Maoz D., Filippenko A. V., Leonard D. C., Matheson T., 2002, PASP, 114, 833
Quimby R. M. et al., 2013, ApJ, 768, L20
Reichardt C. L. et al., 2013, ApJ, 763, 127
Riess A. G., Press W. H., Kirshner R. P., 1996, ApJ, 473, 88
Riess A. G. et al., 1998, AJ, 116, 1009
Riess A. G. et al., 2004, ApJ, 600, L163
Rigault M. et al., 2013, A&A, 560, A66
Rigault M. et al., 2018, preprint (arXiv:1806.03849)
Rodney S. A. et al., 2015, ApJ, 811, 70
Roman M. et al., 2018, A&A, 615, A68
Rosen S. R. et al., 2016, A&A, 590, A1
Rubin D. et al., 2018, ApJ, 866, 65
Sako M. et al., 2018, PASP, 130, 064002
Santos J. S. et al., 2011, A&A, 531, L15
Santos J. S. et al., 2015, MNRAS, 447, L65
Schlafly E. F., Finkbeiner D. P., 2011, ApJ, 737, 103
Scolnic D. M. et al., 2018, ApJ, 859, 101
Silverman J. M. et al., 2012, MNRAS, 425, 1789
Smette A. et al., 2015, A&A, 576, A77
Stalder B. et al., 2013, ApJ, 763, 93
Stritzinger M. D. et al., 2011, AJ, 142, 156
Sullivan M. et al., 2006, ApJ, 648, 868
Sullivan M. et al., 2010, MNRAS, 406, 782
Suzuki N. et al., 2012, ApJ, 746, 85
Tody D., 1986, in Crawford D. L., ed., Proc. SPIE Conf. Ser. Vol. 627, Instrumentation in astronomy VI. SPIE, Bellingham, p. 733
Totani T., Morokuma T., Oda T., Doi M., Yasuda N., 2008, PASJ, 60, 1327
Tripp R., 1998, A&A, 331, 815
Vernet J. et al., 2011, A&A, 536, A105
Webb T. et al., 2015, ApJ, 809, 173
Wilson G. et al., 2009, ApJ, 698, 1943
Wright A. H. et al., 2016, MNRAS, 460, 765
Wu J. et al., 2018, ApJ, 852, 96

SUPPORTING INFORMATION

Supplementary data are available at *MNRAS* online.

Appendix B. Zoomed-in finding charts.

Please note: Oxford University Press is not responsible for the content or functionality of any supporting materials supplied by the authors. Any queries (other than missing material) should be directed to the corresponding author for the article.

APPENDIX A: VLT OBSERVATION LOG

Table A1. See Change transients/host-galaxies observed with the VLT. Note that the exposure time details here refer to the total exposure targeted at an object, whether the data were used or not. The positions here are the calculated position of the transients themselves, rather than the host galaxies.

Transient	Position (J2000)	FORS2 Obs. dates	FORS2 Exp. time (h)	X-Shooter Obs. dates	X-Shooter Exp. time (h)
SCP15A01	$02^h05^m46^s.345$ $-58°28'54''.94$	2016 Sep–2016 Sep 20	2.00	2015 Feb 13–2015 Feb 18	5.00
SCP15A02	$02^h05^m45^s.662$ $-58°28'16''.86$	2015 Oct 4–2015 Nov 10	2.33	–	–
SCP15A03	$02^h05^m44^s.383$ $-58°30'01''.90$	2015 Oct 4–2016 Sep 20	4.33	–	–
SCP15A04	$02^h05^m51^s.130$ $-58°29'27''.38$	2015 Oct 4–2016 Sep 20	4.33	2016 Aug 5–2016 Aug 8	4.00
SCP15A05	$02^h05^m48^s.119$ $-58°29'26''.69$	2015 Oct 4–2015 Nov 10	2.33	2015 Aug 26–2015 Nov 15	4.00
SCP15A06	$02^h05^m43^s.091$ $-58°29'36''.73$	2015 Oct 4–2015 Nov 10	2.33	–	–
SCP15A07	$02^h05^m49^s.295$ $-58°29'41''.02$	2016 Sep 7	0.67	–	–
SCP16A01	$02^h05^m44^s.320$ $-58°29'06''.96$	2016 Sep 7	0.67	–	–
SCP16A02	$02^h05^m45^s.844$ $-58°27'50''.00$	2016 Sep 7–2016 Sep 13	2.00	–	–
SCP16A03	$02^h05^m52^s.390$ $-58°29'40''.28$	2016 Sep 13	0.67	–	–
SCP16A04	$02^h05^m51^s.086$ $-58°29'26''.91$	*Same host as SCP15A04*			
SCP14C01	$10^h14^m04^s.056$ $+00°38'11''.61$	2015 Jan 20	2.71	–	–
SCP15C01	$10^h14^m05^s.174$ $+00°37'16''.39$	2017 Dec 19–2018 Feb 11	4.00	–	–
SCP15C02	$10^h14^m07^s.619$ $+00°38'08''.44$	2017 Dec 19–2018 Feb 11	4.00	–	–
SCP15C03	$10^h14^m07^s.237$ $+00°37'29''.42$	2017 Dec 19–2018 Feb 11	4.00	–	–
SCP15C04	$10^h14^m06^s.530$ $+00°38'47''.08$	2017 Dec 19–2018 Feb 11	4.00	–	–
SCP16C01	$10^h14^m06^s.748$ $+00°39'03''.98$	2017 Dec 19–2018 Feb 11	2.00	–	–
SCP16C02	$10^h14^m08^s.349$ $+00°38'52''.37$	2017 Dec 19–2018 Feb 11	2.00	–	–
SCP16C03	$10^h14^m06^s.374$ $+00°38'25''.36$	–	–	2016 Mar 4–2016 Mar 5	5.00
SCP15D01	$21^h06^m11^s.769$ $-58°45'20''.26$	2016 Jun 30–2016 Jul 2	3.33	–	–
SCP15D02	$21^h06^m07^s.313$ $-58°44'02''.73$	2016 Jun 30–2016 Oct 1	6.67	2015 Sep 18–2016 Jun 30	4.00
SCP15D03	$21^h06^m02^s.299$ $-58°44'54''.03$	2016 Jun 30–2016 Oct 1	6.67	–	–
SCP15D04	$21^h06^m00^s.343$ $-58°45'48''.51$	2016 Jun 30–2016 Oct 1	6.67	–	–
SCP16D01	$21^h06^m07^s.157$ $-58°45'11''.35$	2016 Jun 30–2016 Jul 2	3.33	–	–
SCP16D02	$21^h06^m03^s.439$ $-58°44'16''.01$	2016 Sep 4–2016 Oct 1	3.33	–	–
SCP16D03	$21^h05^m57^s.151$ $-58°45'12''.28$	2016 Sep 4–2016 Oct 1	3.33	–	–
SCP15E01	$20^h41^m04^s.766$ $-44°52'01''.26$	2016 Jun 17–2017 Apr 27	2.00	–	–
SCP15E02	$20^h40^m58^s.767$ $-44°51'02''.55$	2016 Oct 30–2017 Apr 27	1.33	–	–
SCP15E03	$20^h41^m02^s.926$ $-44°51'31''.59$	2016 Oct 30–2017 Apr 27	1.33	–	–
SCP15E04	$20^h40^m59^s.697$ $-44°52'05''.05$	2017 Apr 27–2018 Apr 10	8.00	–	–
SCP15E05	$20^h41^m01^s.123$ $-44°51'12''.21$	2016 Oct 30–2018 Apr 10	7.33	–	–
SCP15E06	$20^h40^m57^s.739$ $-44°51'06''.52$	2016 Oct 30–2018 Apr 10	9.33	–	–
SCP15E07	$20^h41^m03^s.306$ $-44°51'39''.47$	2017 Apr 27–2017 Jun 3	4.00	2016 Sep 21–2016 Sep 30	4.00
SCP15E08	$20^h41^m03^s.775$ $-44°51'28''.39$	2017 Jun 2–2018 Apr 10	6.00	–	–
SCP16E02	$20^h41^m05^s.729$ $-44°51'15''.90$	2017 Apr 27–2017 Jun 3	8.00	–	–
SCP15G01	$00^h44^m02^s.946$ $-20°33'49''.71$	–	–	2015 Aug 24–2015 Dec 8	5.00
SCP16H01	$03^h30^m55^s.991$ $-28°42'46''.56$	–	–	2016 Feb 29–2016 Mar 4	4.00
SCP15I02	$02^h24^m27^s.593$ $-03°22'57''.85$	–	–	2016 Aug 31–2017 Jan 1	9.00

[1]*Physics Department, Lancaster University, Lancaster LA1 4YB, UK*
[2]*Finnish Centre for Astronomy with ESO (FINCA), Quantum, Vesilinnantie 5, University of Turku, FI-20014 Turku, Finland*
[3]*Department of Physics and Astronomy, University of Turku, FI-20014 Turku, Finland*
[4]*E. O. Lawrence Berkeley National Laboratory, Berkeley, CA 94720, USA*
[5]*Department of Physics, University of California Berkeley, Berkeley, CA 94720, USA*
[6]*Space Telescope Science Institute, 3700 San Martin Drive, Baltimore, MD 21218, USA*
[7]*Humboldt-Universität zu Berlin, Institut für Physik, Newtonstrasse 15, D-12589 Berlin, Germany*
[8]*DIRAC Institute, Department of Astronomy, University of Washington, 3910 15th Ave NE, Seattle, WA 98195, USA*
[9]*The Oskar Klein Centre, Department of Physics, AlbaNova, Stockholm University, SE-106 91 Stockholm, Sweden*
[10]*The Research School of Astronomy and Astrophysics, Australian National University, Canberra, ACT 2601, Australia*
[11]*Instituto de Física Fundamental, Consejo Superior de Investigaciones Científicas, c/. Serrano 121, E-28006 Madrid, Spain*
[12]*Institut de Ciències del Cosmos (UB-IEEC), c/. Martí i Franques 1, E-08028 Barcelona, Spain*
[13]*Sorbonne Université, Université Paris Diderot, CNRS/IN2P3, Laboratoire de Physique Nucéaire et de Hautes Énergies, F-4 Place Jussieu Paris, France*
[14]*Sorbonne Universiés, Institut Lagrange de Paris (ILP), 98 bis Boulevard Arago, F-75014 Paris, France*

This paper has been typeset from a TEX/LATEX file prepared by the author.